UNIVERSITY OF OULU

FACULTY OF INFORMATION TECHNOLOGY AND ELECTRICAL ENGINEERING

DEGREE PROGRAMME IN WIRELESS COMMUNICATIONS ENGINEERING

MASTER'S THESIS

THz BAND MULTIPATH MEASUREMENTS AND ANALYSIS

Author	Md Nahiduzzaman
Supervisor	Adj. Prof. Dr. Janne Lehtomäki
Second Examiner	Dr. Sc. (Tech) Joonas Kokkoniemi

May 2020

Nahiduzzaman M. (2020) THz Band Multipath Measurements and Analysis. University of Oulu, Faculty of Information Technology and Electrical Engineering, Degree Programme in Wireless Communications Engineering. Master's Thesis, 56 p.

ABSTRACT

The THz band is now becoming the core interest for many researchers as it offers massive bandwidth and high transmission rates. It is expected to be a solution to ongoing spectrum scarcity in the wireless communication world. Wave propagating through a channel is affected by various phenomena, especially in the case of non-line-of-sight (NLOS) condition. In this thesis work, measurement results on several NLOS propagation mechanisms such as reflection, diffraction, and penetration have been reported in the terahertz band ranging from 0.1 THz to 3 THz. Here, the primary focus is to measure the possible NLOS multipath, such as reflected, diffracted, and penetrated paths or a combination of multiple NLOS components. The goal is to evaluate and analyze the feasibility of those multipath in order to estimate the possibility to establish a communication link via such paths.

The measurements have been conducted by using TeraView TeraPulse 4000, a measurement device that is based on THz time-domain spectroscopy (THz-TDS). Measurements were made under various NLOS propagation scenarios with several common indoor materials. Characteristics of the measured materials have also been reported. The results have been given as a function of frequency and measurement angles.

Corresponding background theories and comparisons with the measurement results have also been investigated with subsequent analysis to check the relevance of the measurement results. The idea was to find possible multipath signals after various NLOS events while traveling through a channel and behavioural changes of the transmitted signal with the change of measurement scenarios. The measurement results agreed with the corresponding theories as expected. The THz band offers overall a decent NLOS wireless communication link between the receiver and transmitter at the lower angles.

Keywords: THz band, reflection, diffraction, penetration, NLOS, multipath measurements.

TABLE OF CONTENTS

FOREWORD

This thesis has been carried out as a partial requirement for the completion of the master's degree program in Wireless Communication Engineering at the Center for Wireless Communication (CWC), University of Oulu.

I would like to take this opportunity to express my heartiest gratitude to my supervisor Adjunct Professor Dr. Sc. (Tech) Janne Lehtomäki for his valuable comments and suggestions from the summer internship to completion of my master's thesis. It has been an honor for me to work with him as a student. I would like to especially thank my second examiner Dr. Sc. (Tech) Joonas Kokkoniemi, for giving me this opportunity to complete my master's thesis under his supervision. I am grateful for his continuous guidance and valuable comments not only on theoretical matters but also for the technical support. His continuous suggestions and comments help me to improve my writing. I have learned a lot from him during this journey. It was one of the most precious experiences of my life.

My special thanks to my parents for giving me permission to pursue my master's degree in Finland. Without their support, it would not have been possible. I would also like to thank my brother Nafi Uz Zaman Shakib, all my friends living here and in my home country for their continuous moral encouragement and support throughout my studies.

Oulu, May 14, 2020

Md Nahiduzzaman

LIST OF ABBREVIATIONS AND SYMBOLS

4G	fourth-generation
5G	fifth-generation
DL	downlink
EM	electromagnetic
eMBB	enhanced mobile broadband
eV	electron volt
FSPL	free space path loss
Gbps	gigabit per second
GHz	gigahertz
HITRAN	high-resolution transmission molecular absorption
IMT	international mobile telecommunication
IoT	internet of things
ISI	inter-symbol interference
IUT	international telecommunication union
LOS	line-of-sight
LTE	long-term evolution
MDF	medium density fiberboard
NLOS	non-line of sight
ps	picosecond
QoS	quality of service
Rx	receiver
SNR	signal to noise ratio
Tx	transmitter
Tbps	terabit per second
THz	terahertz
THz-TDS	terahertz time-domain spectroscopy
UL	uplink
UHF	ultra-high frequency
UWB	ultra-wideband
VNA	vector network analyzer
WPAN	wireless personal area network
WLAN	wireless local area network

c	speed of light
$C(v)$	Fresnel cosine integral
cos	cosine
dB	decibel
d_1	distance from Tx to sample
d_2	distance from the sample to Rx
fs	femtoseconds
f	frequency
f_d	doppler spread
exp	exponential
$G_a G_b$	antenna gain of two antennas
$H(f)$	frequency response
$h(t)$	channel impulse response

$H_c(f)$	power transfer function
$H_s(f)$	sample power transfer function
$H_{sc}(f)$	channel power transfer function
h	height
I	received radiation intensity
I_0	incident radiation intensity
k	absorption coefficient
k_p	penetration coefficient
ln	log base exponential
L_A	molecular absorption loss
L_T	total attenuation
L_{tot}	total path gain
L_{FSPL}	free space path loss
N_{sc}	noise of the sample measurement,
N_c	noise of the reference measurement
n_1	refractive index of air
n_2	refractive index of dielectric material
$P_{Rx(f,r)}$	received power
$P_{Tx(f,r)}$	transmitted power
r	distance
R	reflection coefficient
R_s	the reflectance for the s-polarized light
R_p	the reflectance of the p-polarized light
sin	sine
$S(v)$	Fresnel sine integral
$S_{sc}(f)$	received signal power
$S_c(f)$	reference signal power
T_c	coherence time
v	Fresnel parameter
x	length of LOS path
$X(f)$	transmitted signal spectrum
$x(t)$	transmitted signal
$Y(f)$	received power spectrum
$y(t)$	received signal

α	slit width
β	phase difference
λ	wavelength
θ	diffraction angle
θ_i	angle of incidence
θ_r	angle of reflection
θ_t	angle of transmission
τ	transmittance
μ_1	permeability
μ_2	permittivity

1 INTRODUCTION

The demand for mobile data traffic is significantly increasing day by day. At the same time, the wireless data rates of wireless communication networks are also increasing with the development of communication technologies. Nowadays, people are consuming more and more data in their day to day life with a set of diverse devices that are continuously connected to the internet [1], [2], [3]. That causes slower connections because of lesser bandwidths allocated to each user. Furthermore, the evolvement of user applications over the years in wireless networks now requires high data rates to provide better user experiences and quality of service (QoS). It can be assumed that in the next few years, the existing cellular communication systems will face lack of bandwidth because of the excessive amount of devices connected to the internet [1]. It is expected that the wireless data rates for the 5G technology can be over 10 gigabits per second (Gbps) [3]-[4]. The 5G minimum requirements described in International Telecommunication Union report (IMT-2020) that peak data rates of 20 Gbps downlink (DL) and 10 Gbps uplink (UL) required to support enhanced Mobile Broadband (eMBB) use case scenario [5]. Edholm's law of data rates suggests that if this trend continues, then 100 Gbps data rates can be achieved in the next few years [3]. In order to go beyond 5G peak data rates, higher bandwidths are needed for the upcoming wireless communication systems. To meet up this challenge and to fulfill the demand of higher and reliable data links are one of the most talked topics in the world of wireless communications. The next possible candidate in the electromagnetic spectrum is the unused and unregulated the THz band regime (0.1-10 THz) [6]. Wireless terabit-per-second (Tbps) links are expected to be reality in the future wireless communications [1]-[3], [6]. The THz band might be an excellent option for the wireless communications services beyond 5G. The THz band technologies are now getting enormous attention both in academia and telecommunication industry [7].

1.1 Background and Motivation

The existing modern cellular systems are using frequencies below 6 GHz [9]-[10]. The ultrahigh frequency (UHF) band (300 MHz- 3 GHz) has been heavily implemented. The frequency band allocated for the 4G LTE-Advanced networks are in the range from 600 MHz to 3.5 GHz [9]. Thus, it is getting tougher to allocate this limited frequency spectrum to the ever-growing data traffic in recent times. The 5G networks are expected to use the sub-6 GHz band and the millimeter wave band (30 GHz to 300 GHz) for future wireless communications technology [7]-[8]. The frequency over 100 GHz is very promising because of the very large bandwidths available at the higher frequencies. The THz waves are electromagnetic waves that fall between microwaves and infrared frequencies in the electromagnetic spectrum [7]. The terahertz band generally covers the frequency range from 100 GHz to the far-infrared region (up to 10 THz). This spectrum is sometimes called submillimeter band. This is a massive bandwidth that could be used to overcome the current frequency spectrum scarcity of the wireless communications system [10]-[11]. In the electromagnetic spectrum, radiation at 1 THz has a period of 1 ps, a wavelength of 300 μm, a wavenumber of 33 cm^{-1}, and a photon energy of 4.1 meV [13]. Because of the short wavelengths, the THz waves mostly suffer from attenuation caused by the molecular absorption on water vapor and oxygen in the atmosphere [11]. Also, the free space path loss is in effect. The molecular absorption is responsible for frequency selective fading to the signals. The electromagnetic waves lose energy, which is absorbed mostly by the water vapor in the atmosphere. The absorption loss and free space path loss are also dependent on the distance between the transmitter and the receiver. The molecular absorption loss gets

exponentially higher, and free space path loss increases with the square of the distance [14]. For that reason, the THz band waves are not suitable for long-range radio communications unlike for example microwaves, which have relatively low frequencies, unless very high gain antennas are used [11].

Furthermore, the shortage of bandwidths in the existing communication technology limits desirable data rates. On the contrary, the large bandwidths of the THz band make it very promising to transmit massive amounts of data at a time [11]. The THz frequency band theoretically offers terabit-per-second data capacity as mentioned before [6]. These links are expected to become a reality in the upcoming years. To support the ever-growing data traffic, as a possible solution, new spectral bands should be introduced. The THz band might be considered as a possible solution for both macroscale and nanoscale communications. Macroscale networks are such as WPAN, WLAN, cellular networks [6]. Nanoscale communications consist of nanoscale interconnected networks that can perform data processing and storage, computing, sensing, or actuation [6]. That could provide opportunities to establish communications within nanoscale devices such as sensors or actuators. These nanoscale sensors can continuously transmit the sensing data to the existing wireless sensor networks. Moreover, these impressive short-range opportunities can offer a great prospect for the Internet of Things (IoT) applications as well. The relation between these nanoscale devices with the classic wireless networks sometimes refers to as the Internet of nano-things [12]. The THz band is also used in imaging and sensing applications. It can also be used to communicate for intra-body wearable nano-bio-sensing networks and the detection of harmful chemicals. This nanoscale communication is possible due to very small-sized nano antennas that allow communication in high frequencies [6].

The THz band offers large bandwidths but with a cost of high path loss in the THz channel. That is one of the main shortcomings of the THz frequencies. Line-of-sight (LOS) communication might be the best way to establish a communication link in terahertz due to its relatively short range. The THz band can provide small cells with ultra-high-speed data in LOS between Tx and Rx [5]. Nevertheless, the recent studies from various researchers have suggested that the non-line-of-sight (NLOS) propagation can also be considered for the THz band communication [14]-[21]. The aim of this thesis work is to examine the possible NLOS phenomena of the THz band. It is necessary to analyze the THz channel theoretically and empirically.

To understand the NLOS phenomena in the possible multipath environment, we designed several propagation models and conducted multiple measurements to validate our experiment with the corresponding theoretical model. We also revisit several earlier research papers to widen our knowledge on this topic. Various NLOS propagation phenomena such as reflections, diffractions, penetrations are studied individually, and also a combined experiments of two single NLOS phenomena have been performed and evaluated through numerical analysis. The received responses at the receiver have been summed up to get the combined multipath responses. The primary objective of this work was to find the feasibility of the combined multipath signal at the receiver. Besides that, the possibility of such paths to establish communication in terahertz frequencies.

This thesis work also presents the results of the refractive index and the penetration coefficient of various dielectric materials in order to model the NLOS propagation models discussed above.

1.2 Organization of the Thesis

This thesis work is organized as follows, in this first chapter, a brief introduction is given, and background of the THz band is discussed. In Chapter 2, a literature review of previous scientific research papers on the possible communication channel model through NLOS propagation of the THz wave is evaluated. In Chapter 3, the related theory of electromagnetic wave propagations, terahertz channel theoretical models are studied. Chapter 4 gives a concise overview of the measurement device, measurement setup, and scenarios for the simulation models along with the introduction of the materials used in the measurements. Chapter 5 evaluates the measurement results and subsequent analysis of the thesis work. The conclusion and discussion are given in the final chapter of this master's thesis.

2 LITERATURE SURVEY

In the terahertz band communication, the LOS between transmitter and receiver is an important feature and preferable for lowest possible channel loss. However, NLOS propagation phenomena, including reflections, diffractions, and penetrations, provide opportunity to communicate through multiple paths. There are many research papers that show good agreement between theoretical and measured results, mostly focused on the lower portion of the terahertz band such as [14]-[19] & [21].

The penetration properties of different materials in the THz frequency has been studied in several papers. For example, [15], [16] mainly focus on the penetration properties of common indoor materials such as glass, hardboard, plastics, and paper. These papers were used to develop our model to study the penetration properties of dielectric materials. The study shows that the penetration is only possible at the lower end of the THz band. The loss is significant at the higher end of the THz band. Thus, frequencies above one terahertz are not very suitable to communicate through different objects. The findings in the above mentioned papers were that the penetration loss of the received signal increases with the increase of incident angle. It also depends on the thickness of the materials. The frequency response of the higher frequencies is most likely filtered out due to increasing loss and due to pulse shape, that has less energy on the higher frequencies. The NLOS communication always causes an additional delay to the signal since the refractive index of the material is higher than one of the air. The NLOS paths through different materials can cause inter symbol interference (ISI). Both papers concluded that NLOS communication is still challenging in the higher portion of the terahertz band. However, a decent possibility is inevitable at the lower end of the THz band. Thus it can be possible to communicate through the penetrated path in the THz region to some degree [15], [16].

Most of the literature on the THz band is focusing on reflections and scattering measurement techniques and possible communication link via multipath. By using these NLOS phenomena, it is very much possible to establish communication links between Rx and Tx at such high frequency. A wide range of these papers is concentrated on both theoretical and measurement perspectives. For instance, [14], [17] and [18] shows good agreement with the theoretical models and measured values. In particular [14] and [18], concentrate on studying the rough surface scattering phenomena and the characteristics of the reflected and scattered THz radiation in the frequency domain, whereas in papers [17] and [18], measurements were conducted around 300 GHz, the lower end of the THz band.

The work in [14] presents scattering and reflection properties of different common indoor materials in the frequency domain by making the NLOS propagation model, and ray tracing was used to model a link between the transmitter and receiver. The ray tracing model is a very good tool to calculate the radiated paths. The measurements in [14] are very much related to our work. The measurements were performed by THz-TDS based measurement device and the measurements were taken from 0.1 to up to 4 THz. This paper shows the frequency responses of those samples by varying the Tx and Rx from different angles and also presented a comparison between various materials. The path gain is used to evaluate the quality of the channel in some particular conditions. The reflected path offered decent responses up to 2 THz. Some samples offer decently good frequency responses. Notably, aluminum is an excellent reflector amongst the glass, plastic, hardboard, and concrete. However, the response of the glass and plastic samples are slightly better than aluminum in certain frequencies, specifically between 1.5 and 2 THz. The concrete sample, which was the roughest among them all, proved to have good scattering properties in their experiment. The authors found that diffuse scattering

has a minimal contribution in comparison to the specular reflected components. Although, in some cases, the diffuse scattering has a high intensity to enable NLOS communication, and it mostly depends on the surface roughness as well as the frequency. However, it is necessary to know the reflectivity of the materials to create the geometrical propagation simulation or ray tracing model.

In [17], the authors studied both reflection and knife-edge diffraction effects at 300 GHz, and they showed an excellent agreement between the measurement results and corresponding theories. The authors also gave an estimation of a path loss model based on their measurements and reported channel transfer functions in the paper. The measurements were carried out for two individual indoor scenarios to present ultra-broadband channel measurements at 300 GHz. The measurements were conducted by VNA (Vector Network Analyzer) with regard to distance, different antenna types, and device displacements. A short-range desktop and small indoor office scenario (longer range) were utilized to make the channel measurements. The authors noted that the two open-ended waveguides can only be operated in a short distance up to 10 cm. This is caused by the fact that there is no antenna if the waveguides are open ended. The authors also experimented interference behaviour according to the two ray model. Highly directive antennas have been used to conduct measurements and thus a slight displacement may cause a severe attenuation of the signal. The author concludes by saying that ultra-broadband channels at 300 GHz give almost flat channel transfer functions for both LOS and NLOS situations. Directed NLOS paths can be considered for communication regardless of the higher attenuations. Diffuse scattering from rough surfaces around 300 GHz was also investigated in [18]. The paper verified that the Kirchhoff's theory of scattering is valid method to model the THz band scattering. Diffuse scattering from the materials existing in the indoor locations has a significant impact on such high frequencies. The simulation results by using a ray tracing algorithm in [18] show that diffuse scattered power has a significant influence on NLOS propagation paths. However, scattering from rough surfaces reflected in different directions in practical scenarios. On the other hand, specular reflection component is much more significant for NLOS communication, as it contains directly reflected paths with the most energy.

Papers [19], [20] present the frequency dependent refractive index and the absorption coefficient results of commonly used materials from 100 GHz to 1 THz frequency range. The authors suggest that the results of the absorption coefficient are useful to calculate the attenuation of a penetrated paths.

Diffraction is another significant NLOS propagation phenomenon that is important to study in order to investigate signal propagation in future THz systems. The knife-edge diffraction effect is more common in communications than the slit diffraction. Papers [17], [21] studied diffraction effects and different measurement techniques in the THz band frequency. Our work is also partially based on paper [21]. This scientific paper shows that the diffracted path can be used to set up communication links in the THz band even in the shadow regions of the objects. Diffraction mostly occurs at the edges, and the edges operate as secondary sources for the radiation. Two types of diffraction were taken into account in [21]. Knife-edge diffraction with finite thickness and two slit diffraction have been studied. These measurements were also carried out by TeraView TeraPulse 4000 measurement device within the bands from 100 GHz to 2 THz. A two millimeter thick aluminum sheet was used to measure the knife-edge effect. In the THz wavelengths, the two millimeter thickness forces to study the round knife-edge diffracted intensities. The results show the path gains (dB) as a function of frequency and diffraction angle. From the data analysis, it is shown that with the increase of angle, the path gains decays exponentially. The paper concludes that single slit diffraction shows lower

attenuation in comparison to the knife-edge effect. The slit diffraction model can be used as a multipath communication model with a considerably high transmit power.

Furthermore, it is crucial to calculate the reflections, scattering, diffraction, and penetration losses to estimate the overall terahertz wave communication channel. All the papers discussed above suggest that the communication in the THz frequency via different multipath in the NLOS situation is possible with certain limitations.

3 WAVE PROPAGATION MECHANISM

Wave propagation refers to the propagated path in which the wave travels in a communication channel. Here, in this chapter, the basic propagation phenomena will be discussed with related theories emphasizing the THz band signal propagation. In a multipath propagation channel, the signal propagates between the transmitter and receiver through several different paths. When a signal experiences dielectric obstacle in a communication channel, it can be either reflected from a smooth surface or diffusely scattered from a rough surface. It can also be penetrated through different objects or sometimes diffracted from the sharp edges of dielectric objects before received by the receiver [43]. These propagation phenomena play a significant role in establishing communication through multipath in NLOS channels. Due to the high path loss of the THz band signal, it is the obvious choice to establish LOS communications between the Tx and Rx. The most challenging part is to deal with the considerable path loss that occurred in this very high-frequency band due to its distinct features. Free space path loss (FSPL) and molecular absorption losses are considered significant losses in the terahertz band communication. It is not always possible to secure LOS path between the Tx and Rx. Despite all of that, it can be very much possible to establish a communication path in NLOS in short-range communication. This chapter includes all the necessary background theories of the THz band wave propagation related to our work.

3.1 Molecular Absorption Loss

There are several challenges to establish possible communication at the THz frequencies. One of the primary problems is the very high propagation loss, which limits the distance between the transmitter and receiver. The free space path loss and molecular absorption loss makes the communication very challenging in the THz band [31]. In this subsection, we focus on molecular absorption loss. The other significant phenomenon, the FSPL is discussed in Section 3.2.

The THz band is very sensitive to humidity changes due to its strong attenuation by water vapor. In the THz band communication, a propagating wave can be attenuated greatly due to this molecular absorption when traveling through a wireless channel. The maximum communications range maybe just a few meters with low gain antennas [14].

This attenuation is caused due to some part of wave energy is converted into internal and kinetic energy of the molecules in the communication channel [31]. It is necessary to compute the frequency dependent absorption coefficient $k(f)$ to compute the molecular absorption loss. The absorption coefficient varies with pressure and temperature in the environment. The information to calculate it available in the HITRAN database [22]. The amount of incident radiation that is capable of passing through an absorbing medium can be obtained from the transmittance, τ of that medium. The transmittance can be derived by using Beer-Lambert's law [23], [32], [33]

$$\tau(f,r) = \frac{P_{Rx(f,r)}}{P_{Tx}(f,r)} = e^{-k(f)r}, \tag{1}$$

where $P_{Rx(f,r)}$ and $P_{Tx(f,r)}$ are the received and transmitted power respectively, r is the distance between the transmitter and the receiver.

Molecular absorption loss, L_A of a certain frequency, f can be expressed as [23], [32]

$$L_A(f,r) = \frac{1}{\tau(f,r)}, \tag{2}$$

$$L_A(f,r) = \mathrm{e}^{\mathrm{k}(f)\mathrm{r}}. \tag{3}$$

3.2 Free Space Path Loss

FSPL is the attenuation in signal strength when propagating in the LOS path through free space between two antennas. In this case, the propagating wave does not experience any obstacles. This phenomenon is needed to take into account since it is always in effect in the wireless channel. The FSPL gives a very good approximation about the attenuation of the signal traveling in the free space or air (when the FSPL is combined with molecular absorption loss introduced in Section 3.1). The FSPL can be above 100 dB for a 10-m link at the THz frequencies [31]. The FSPL can be derived from the Friis transmission formula which state as [25]

$$\frac{P_{Rx}}{P_{Tx}} = G_{Tx}G_{Rx}\left(\frac{\lambda}{4\pi r}\right)^2, \tag{4}$$

considering the power input of the transmitter antenna is P_{Tx}, λ is the wavelength and the received power is P_{Rx}. Here, G_{Tx} and G_{Rx} are the maximum antenna gain of the transmitter and the receiver antenna, respectively.

For isotropic antennas, the FSPL can be expressed as [25]

$$L_{FSPL} = \frac{P_{Tx}G_{Tx}G_{Rx}}{P_{Rx}} = \left(\frac{4\pi r}{\lambda}\right)^2 = \left(\frac{4\pi rf}{c}\right)^2, \tag{5}$$

where r is the distance between the two antennas, c is the speed of light and f is the frequency.

The total attenuation loss can be calculated by using the following equation,

$$L_T = L_A \,.\, L_{FSPL}. \tag{6}$$

3.3 Noise

Noise in a wireless communication channel can be defined as any response or energy which causes attenuation or degradation of the quality to the transmitted message signal. A signal can be affected by different types of the noise source in a wireless channel. Traditional noises like thermal noise in the receiver component and radio noise also degrade signal strength in the THz band communication. Electronic components always caused noise in the radio system. The thermal noise is caused by the thermal motion of the electrons in the receiver electronics. The thermal noise is white noise. Its power depends on the absolute temperature of the receiver and the bandwidth. The thermal noise remains constant over frequency since it is white noise [45]. There is also ambient noise from the existing environment, which may increase the noise level a bit in the THz communication channel. It is based on the sky noise. It is a source of systematic noise caused by variations in atmospheric emissivity. This is one kind of radio noise that is received by the receiver from the atmosphere or the sky [31].

3.4 Fading

Fading is a common phenomenon in the communication channel, especially in multipath propagation. Multipath is the propagation phenomena where Rx receives the transmitted signals through multiple different paths. There are multiple replicas of the message signal received by the receiver based on the superposition principle. With the moving Tx and Rx, this multipath phenomenon can be time-varying, and fading occurs. The fading is caused by the constructive and destructive interference of the delayed and attenuated signal propagated through the aforementioned different multipath [27].

Multipath fading can be modeled statistically. The Rayleigh model is used to describe the behaviour of the fading when LOS channel does not exist. If there is a strong path among weaker ones, then the fading is often modeled according to Rician fading to approximate the signal behaviour. This typically happens in the case of LOS [28]. Fading can occur both in the time and frequency domain. The received signal can experience both fast and slow fading (shadowing). These phenomena depend on the coherence time. Whereas the coherence time is related to the Doppler spread, f_d by [29]

$$T_c \cong \frac{1}{f_d}. \tag{7}$$

If the delay requirement is longer than the coherence time T_c, then the channel is referred to as fast fading. Otherwise, it is said to be slow fading if coherence time T_c is greater than the delay requirement. Slow fading can occur in the wireless channel due to shadowing by some objects between the transmitter and receiver. Frequency flat and frequency selective fading are also common characteristics in fading channels. Frequency flat or frequency nonselective is a phenomenon in narrowband systems. When the coherence bandwidth is larger than the bandwidth of the signal, flat fading occurs. Frequency selective fading occurs in wideband systems where the coherence bandwidth is smaller than the bandwidth of the signal. In this type of fading, spectral components of the modulated signal are affected by the different amplitude gains and phase shifts [29]. Due to the short wavelength of the THz band, the fading can be very fast in the moving objects. However, Rician or Rayleigh fading is unlikely because of the directive antennas that reject most of the multipath components. Hence, in the THz band, the frequency selective fading in LOS conditions can occur due to the molecular absorption, but in NLOS are also dependent on the NLOS loss mechanisms.

3.5 Polarization

Polarization typically applies to transverse waves that describe the electric field orientation. It is a distinct characteristic of all transverse waves that specifies the geometrical orientation of the wave. The electromagnetic wave consists of two oscillating vector fields; electric and magnetic field. These two vector fields are perpendicular to each other. The direction of the polarization of an electromagnetic wave always refers to the direction of the electric field vector [26]. The alignment of the electric field vector to the direction of propagation defines the polarization of waves [25]. It may be classified into three categories, such as linear, circular, or elliptical polarization [41]. If the electric field vector has a single direction along with the propagation axis or oscillates only in one line, it can be termed as linearly polarized. It can be subcategorized into vertical and horizontal linear polarization. If the electric field vector rotates in a circle around the direction of propagation with a constant magnitude, then the wave can be termed as circularly polarized (CP). It can be subcategorized as left or right hand-polarization,

depending on the direction of rotation. Linear and circular polarization are special cases of elliptical polarization [25], [41], [42]. In elliptical polarization, the electric field vector rotates elliptically with varying amplitudes about the direction of propagation [25]. The circular and elliptical polarization differs in such a way that in the case of elliptical polarization, the two linear components which are perpendicular to each other can have the same or different magnitude, whether in circular polarization both linear components have to be in the same magnitude. It is essential to analyze the polarization properties of electromagnetic waves to understand the plane wave incidence of electromagnetic waves properly.

3.6 Reflection and Refraction

The study of reflection properties is very important and common in the wireless communication channel. Figure 1 represents a plane wave incident onto a plan boundary. When a plane wave encounters onto a plane boundary between two media with different permeability (μ_1, μ_2) and permittivity $(\varepsilon_1, \varepsilon_2)$, then two phenomena may occur. In this case, both media are assumed to be lossless or ideal. One wave can propagate within the first media but moves away from the plane wave boundary and makes an angle θ_r to the normal, and this is called the reflected wave. The other wave which can propagate into the second medium and makes an angle θ_t to the surface normal is called the transmitted or refracted wave. The later mechanism is called refraction [25].

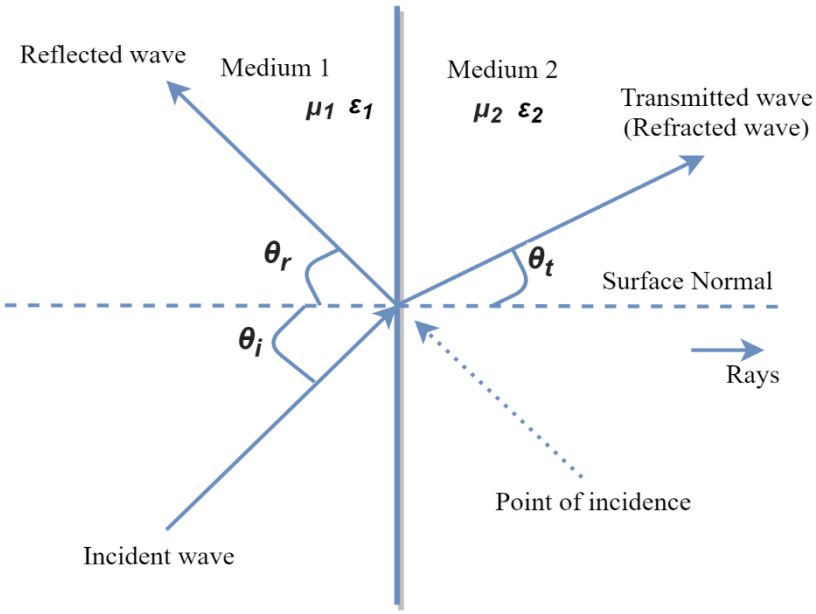

Figure 1. Plane wave incident onto a plane boundary.

Snell's law of reflection suggests that the angle of the reflected ray is related to the incidence angle as

$$\theta_i = \theta_r, \tag{8}$$

where θ_i is known as the angle of the incidence. Snell's law of refraction can be expressed as

$$n_1 \sin \theta_i = n_2 \sin \theta_t, \tag{9}$$

where n_1 and n_2 are the refractive index of the different mediums. In our experiment n_1 is the refractive index of air, and it is assumed to be one, and n_2 is the refractive index of the different used materials in the measurement. The information about the materials is discussed in the later chapter [25].

In our experiment, the dielectric materials have been used to conduct our measurements. When a wave travels in a communication channel and encounters a dielectric material then part of that wave will be refracted by the material, and part of it will be reflected back to the receiver. The well-known Fresnel equations give information about the amplitude and phase of the reflected and transmitted components. This also depends on the refractive index of the material and angle of incidence of the wave to the material. In the THz frequency, the refractive index of the material is unknown in most cases, due to the frequency dependence of the refractive indices [16], [38]. In our experiment, we try to find out the refractive indices of the different materials used in our measurements over different frequency ranges. In order to find the refractive index in the lower portion of the THz region. The refractive index of air is assumed one which stated earlier and then we evaluate the material refractive indices over a span of frequencies from 300 GHz to around 900 GHz [19].

The Fresnel equations are as follows. The total reflection coefficient, $R(\theta_i)$ for circularly polarized radiation is [39]

$$R(\theta_i) = \frac{1}{2}\big(R_s(\theta_i) + R_p(\theta_i)\big), \tag{10}$$

Where

$$R_s(\theta_i) = \left|\frac{n_1 \cos\theta_i - n_2 \cos\theta_t}{n_1 \cos\theta_i + n_2 \cos\theta_t}\right|^2, \tag{11}$$

or

$$R_s(\theta_i) = \left|\frac{n_1 \cos\theta_i - n_2\sqrt{1-\left(\frac{n_1}{n_2}\sin\theta_i\right)^2}}{n_1 \cos\theta_i + n_2\sqrt{1-\left(\frac{n_1}{n_2}\sin\theta_i\right)^2}}\right|^2, \tag{12}$$

And

$$R_p(\theta_i) = \left|\frac{n_1 \cos\theta_t - n_2 \cos\theta_i}{n_1 \cos\theta_t + n_2 \cos\theta_i}\right|^2, \tag{13}$$

or

$$R_p(\theta_i) = \left|\frac{n_1\sqrt{1-\left(\frac{n_1}{n_2}\sin\theta_i\right)^2} - n_2 \cos\theta_i}{n_1\sqrt{1-\left(\frac{n_1}{n_2}\sin\theta_i\right)^2} + n_2 \cos\theta_i}\right|^2, \tag{14}$$

where $R_s(\theta_i)$ is the reflectance for the s-polarized light and $R_p(\theta_i)$ is the reflectance of the p-polarized light. The polarization of the measurement device was unknown in our case. We tried to adjust the polarization with a 97% s-polarized radiation and 3% p-polarization radiation to fit the measured reflection coefficient to the Fresnel equations [19]. The results are given in Section 5.3.

3.7 Penetration Loss

In the electromagnetic spectrum, the THz waves are placed between microwaves and infrared waves. Thus, the THz waves have shorter wavelengths than microwaves and longer than visible and infrared waves. Electromagnetic wave incidents on a particular material have several phenomena such as the wave that can be reflected, scattered from the surface, or diffracted from the edges of the materials, as discussed earlier. One of the properties of the THz waves is transparency to different dry dielectric materials. These waves can easily penetrate clothes, different types of papers, wood, glass, and plastics [13]. This penetration property of the THz waves offers a good opportunity to communicate through these existing materials in indoor locations. It provides a very good possibility to create an NLOS communication link through penetration from material between a transmitter and a receiver. The behaviour of the wave inside a material depends on the characteristics and thickness of that specific material. This measure is called penetration depth [34]. The path loss increases linearly with the increase of the thickness of the materials. This phenomenon always provides an additional delay to the received signal at the receiver as the wave travel longer distances into the material. The THz band uses short pulses so that this delay might influence the detection in the receiver [16]. This delay also dependent on the refractive index of a material.

To investigate the path loss of a transmitted path after the penetration from a material, we need the information of penetration coefficients of that material. This penetration coefficient can be calculated from the Beer-Lambert's law, discussed in Section 3.1. Here, the penetration coefficient $k_p(f)$ is [16], [17]

$$k_p(f) = -\frac{\ln\left(10^{\frac{H_{dB}(f)}{10}}\right)}{r}, \tag{15}$$

where $H_{dB}(f)$ is the path gain of a particular sample, given in dB-scale and r is the thickness of that individual sample. The path gain can be calculated by (1),

$$\tau(f) = \exp\left(-k_p(f)r\right), \tag{16}$$

here $\tau(f)$ is the transmittance or path gain at an arbitrary distance r inside that particular material [16].

3.8 Diffraction

Diffraction refers to a phenomenon in which the waveform bends around the corner or sharp edges when it encounters an obstacle. Some energy does propagate in the shadow region when passing through an aperture or slit. This is another natural phenomenon after reflection for which the radio signal actually can propagate in the NLOS channels. This effect of the shadow region of an obstacle can be understood by using Huygens's principle. According to Huygens's principle, every point of a wavefront can be considered as a source of secondary wavelets [26]. The diffracted path is also a significant phenomenon in NLOS multipath environment. The receiver antenna can receive the transmitted signal after experiencing multiple obstacles in the communication channel. As we know, the wavelength is very low in the THz communications; thus, the study of this phenomenon is noteworthy, especially for NLOS communication [25], [21]. In this thesis work, the frequently happened knife-edge diffraction and as well as single

slit diffraction in a radio channel have been studied. The following subsections give an overall view of the theoretical model used to compare and verify the actual measurement data.

3.8.1 Knife-Edge Diffraction Model

The knife-edge diffraction model is used in most practical situations to know the diffraction pattern of the signal better. This phenomenon happens when a wave incident on an obstacle, especially on the sharp or knife-edge of that obstacle, while propagating through a wireless channel. Therefore, the edge act as a secondary source, which allows the wave to propagate into the shadowed region. We model the knife-edge diffraction with a finite width in our experiment, which is discussed very well in [21].

The behavioural pattern of waves can be predicted by the [21]

$$L(\theta) = \frac{\left(1-\mathrm{C}(v)-\mathrm{S}(v)\right)^2+\left(C(v)-S(v)\right)^2}{4}, \tag{17}$$

here θ is the diffraction angle given in Figure 2 and $\mathrm{C}(v)$ and $S(v)$ are the Fresnel cosine and sine integrals given by

$$C(v) = \int_0^v \cos\left(\frac{\pi s^2}{2}\right) ds, \tag{18}$$

$$S(v) = \int_0^v \sin\left(\frac{\pi s^2}{2}\right) ds, \tag{19}$$

the diffraction gain depends on the value of v, the Fresnel parameter given by [36],

$$v = h\sqrt{\frac{2}{\lambda}\left(\frac{1}{d_1}+\frac{1}{d_2}\right)}, \tag{20}$$

where h is the height of the object measured from the LOS path as shown in Figure 2. Based on the measurement setup, the length of the LOS path x can be calculated with the law of cosines as

$$x = \sqrt{d_2^2 + d_1^2 - 2d_1 d_2 \cos(\pi - \theta)}. \tag{21}$$

Angle α can be obtained from the LOS path length as

$$\alpha = \cos^{-1}\left(\frac{d_1^2+x^2-d_2^2}{2xd_1}\right). \tag{22}$$

The height h is calculated by

$$h = d_1 \tan(\alpha). \tag{23}$$

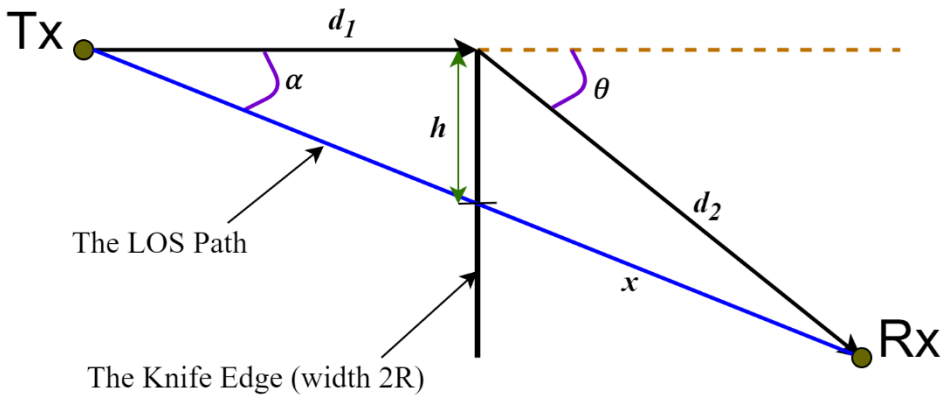

Figure 2. The geometry of knife-edge & slit diffraction measurements technique.

Figure 2 shows the geometry of the two diffraction patterns experimented in our work. The knife-edge in the actual measurement is rectangular. However, due to use of a knife-edge of finite thickness in the actual setup, there is an additional attenuation. That was added by a round obstacle to adjusting the theoretical model with the measured values. The knife-edge of finite thickness is not entirely true knife-edge. Diffraction can happen at both sides of the obstacles and lead propagation along the top of the obstacles. This phenomenon can lead to more attenuation. The signal strength can hardly be predicted accurately in such conditions [37]. Thereinto by adjusting the theoretical model along with the measured values, we also calculated the additional attenuation caused by the round obstacle. It can be assumed here that two consecutive knife-edges are separated from each other by a distance of $2R$, as shown in Figure 2. The diameter, R of an imaginary circle, is assumed to be between the edges. This is half of the knife-edge thickness. From this, we can calculate the additional attenuation to the knife-edge which is given in dB-scale [21], [24]

for $mn \leq 4$, and

$$\mathrm{T}_{dB}(m,n) = 7.2m^{\frac{1}{2}} - (2 - 12.5n)m + 3.6m^{\frac{3}{2}} - 0.8^2\,, \tag{24}$$

for $mn > 4$, where

$$\mathrm{T}_{dB}(m,n) = -6 - 20\log_{10}(mn) + 7.2m^{\frac{1}{2}} - (2 - 17n)m + 3.6m^{\frac{3}{2}} - 0.8^2, \tag{25}$$

where the value of m and n can be obtained by following,

$$m = \frac{R\left(\frac{1}{d_1}+\frac{1}{d_2}\right)}{\left(\frac{\pi R}{\lambda}\right)^{\frac{1}{3}}}, \tag{26}$$

$$n = \frac{h}{R}\left(\frac{\pi R}{\lambda}\right)^{\frac{1}{3}}. \tag{27}$$

Now, the total path gain can be calculated in linear scale as follows

$$L_{tot}(\theta) = L(\theta)10^{-\left(\frac{T_{dB}(m,n)}{10}\right)}. \quad (28)$$

3.8.2 Single Slit Diffraction Model

When electromagnetic wave passing through a slit generally forms a diffraction pattern. In this diffraction pattern, slit acts as a 'virtual' source, which is different from the knife-edge or diffraction gratings. Diffraction can be single slit or multiple slit [26], [21]. In our experiment, herein, only a single slit diffraction pattern is examined, and the measured values are well-matched with the standard slit diffraction theories. This slit diffraction is not as significant as the knife-edge is but still has studied in several scientific papers over the years. This pattern is also can be an option for communication in the NLOS channels. Thus, the signal can be received by the receiver after slit diffraction occurs in the propagation medium. Slit diffraction occurs typically when the wave propagates through a single or multiple slits. Single slit diffraction pattern forms a different diffraction pattern from the multiple slit diffraction. When a wave is passing through a slit, then according to Huygen's principle, each part of the slit can be imagined as an emitter that emits waves or acts as the source of secondary waves like knife-edge [26]. Figure 3 shows the graphical illustration of the slit configurations used in our measurement.

The intensity of a single slit pattern as a function of angle is given by [26].

$$\frac{I}{I_0} = \left(\frac{\sin\left(\frac{\beta}{2}\right)}{\frac{\beta}{2}}\right)^2, \quad (29)$$

where I is the received radiation intensity, I_0 is the incident radiation intensity and the phase difference is given by [26]

$$\beta = \frac{2\pi a}{\lambda}\sin(\theta), \quad (30)$$

where a is the slit width, θ is the diffraction angle and λ is the wavelength.

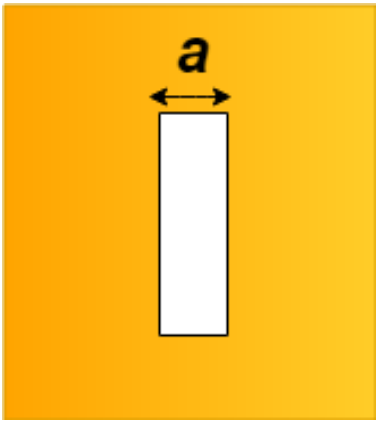

Figure 3. Graphical illustration of single slit diffraction.

3.9 Frequency and Impulse Responses

The channel frequency response is used to describe the channel behaviour as a function of frequency. When multiplying transmitted signal spectrum $X(f)$ by the frequency response $H(f)$, we get the received power spectrum $Y(f)$. In the frequency domain, this can be expressed as [30]

$$Y(f) = H(f)X(f). \tag{31}$$

In the time domain, the channel is described by the channel impulse response $h(t)$. We know that the impulse response is the inverse Fourier transform of the frequency response, hence the received signal $y(t)$ in the time domain can be expressed as

$$y(t) = h(t) * x(t), \tag{32}$$

where $x(t)$ is the transmitted signal and $(*)$ denotes the time-domain convolution of the signals [30]

In our case we calculate the path gains in order to investigate the relative strengths of the received signals after multiple phenomena in the channel. The path gain of the communication channel can be estimated by comparing the frequency domain samples with the reference signal. The frequency domain path gain corresponding to the channel transfer function can be obtained by using the reference signal as [14]

$$\frac{S_{sc}(f)}{S_c(f)} = \frac{H_{sc}(f)X(f)+N_{sc}}{H_c(f)X(f)+N_c} = \frac{H_s(f)H_c(f)X(f)+N_{sc}}{H_c(f)X(f)+N_c} \approx H_s(f) + \frac{N_{sc}(f)}{H_c(f)X(f)}, \tag{33}$$

where $S_{sc}(f)$ is the received signal power through the sample and the channel, $S_c(f)$ is the reference signal power, $H_{sc}(f)$ is the channel power transfer function of the sample and channel, $H_c(f)$ is the power transfer function of the channel only, N_{sc} is the noise of the sample measurement, N_c is the noise of the reference measurement, $X(f)$ is the signal power envelope (unknown), and $H_s(f)$ is the sample power transfer function. The last noise term comes from the assumption that the noise power is small in comparison to the reference signal power [14].

For multipath measurements, following equation has been obtained

$$\frac{S_{s(r.p)}(f)}{S_{c(r.p)}(f)} = \frac{H_{s(r)}(f)H_{s(p)}(f)H_c(f)X(f)+N_{s(r.p)}}{H_c(f)X(f)+N_c} \approx H_{s(r)}(f)\, H_{s(p)}(f) + \frac{N_{s(r.p)}(f)}{H_c(f)X(f)}, \tag{34}$$

here $S_{s(r.p)}(f)$ is the received signal power after multiple phenomena through the sample, $S_{c(r.p)}(f)$ is the reference signal power, $H_{s(r)}$ is the channel power transfer function of the sample after reflection, $H_{s(p)}(f)$ is the channel power transfer function of the sample after penetration and $N_{s(r.p)}$ is the noise component of the multiple sample measurements.

4 MEASUREMENT SCENARIOS

The NLOS phenomena in terahertz band radiation can be analyzed by measuring the possible propagation of multipath signal responses. We analyzed the propagation channel by taking the necessary measurements. The measurements were conducted using a TeraView TeraPulse 4000 measurement device. In this chapter, a brief introduction about the device, materials used to take measurements, and the complete measurement scenarios have been discussed with supplementary photos. The measurements were performed at the laboratory of the University of Oulu.

4.1 Measurement Device

The measurement device TeraView TeraPulse 4000 relies on the THz Time-Domain Spectroscopy (THz-TDS) in the THz band measurements. This device consists of a processing unit, measurement head sensors and two measurement plates. This device can perform reflection, diffraction, and penetration measurements by varying angles. The device is capable of capturing measurements data in the time domain. We used the Matlab software program to observe the frequency domain behaviour of the signal by using Fourier transform. In order to excite the emitter (Tx) and receiver (Rx) antennas of the device, ultra-short laser pulses (~ 100 fs) have been used. This leads the transmitter to emit short laser pulses in the frequency range of THz band. The receiver enables a short time window detection to receive the THz pulses. Therefore, to get the full-time domain pulses, a delay line is used by the device to get the total time domain data. It is enabling the pulse detection one time instant at that specific time frame. Then the transmitted pulse detected and measured by the Rx antenna at that particular time instant. After that, the receiver measures the next time frame [15]. The device beamwidth is approximately 2 cm. There are generally two types of measurement settings, which are low and high-resolution settings. High-resolution settings are appropriate for materials characterization, and low-resolution settings can be used for the averaging of a higher number of measurements and suitable for real-time monitoring of the measured data. The primary aspect of using the device is that it can measure from approximately 100 GHz to almost 4 THz. Figure 4 shows the measurement device in operation while taking the reference signal where the measurement heads are 20 cm apart from each other. The two measurement heads contain the emitter (Tx) on the right side visible in the picture and receiver (Rx) on the left side [14], [16], [21].

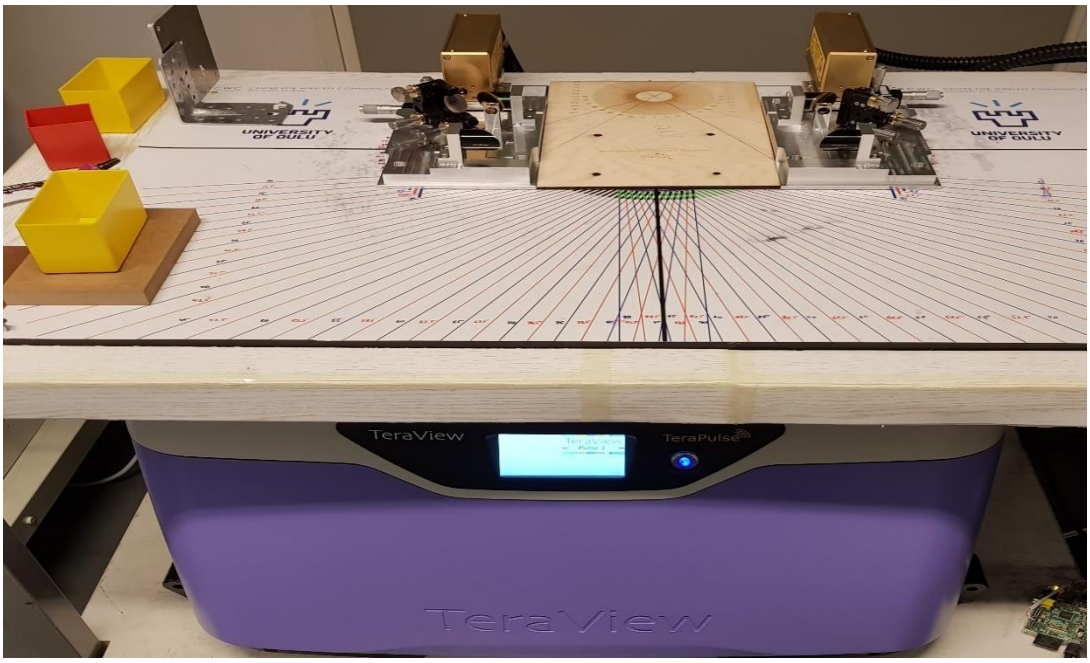

Figure 4. TeraView TeraPulse 4000 measurement device.

Figure 5 presents the pulse shape of the reference signal in the dB scale from 0.1 to 4 THz. The reference response has been taken in full LOS. The Tx and Rx placed in such a way that the gap between the two heads is exactly 20 cm, which ensures enough space to operate the two plates carefully while taking the measurements by using different samples. The sharp spikes at the high frequencies are indicating the absorption lines in the figure.

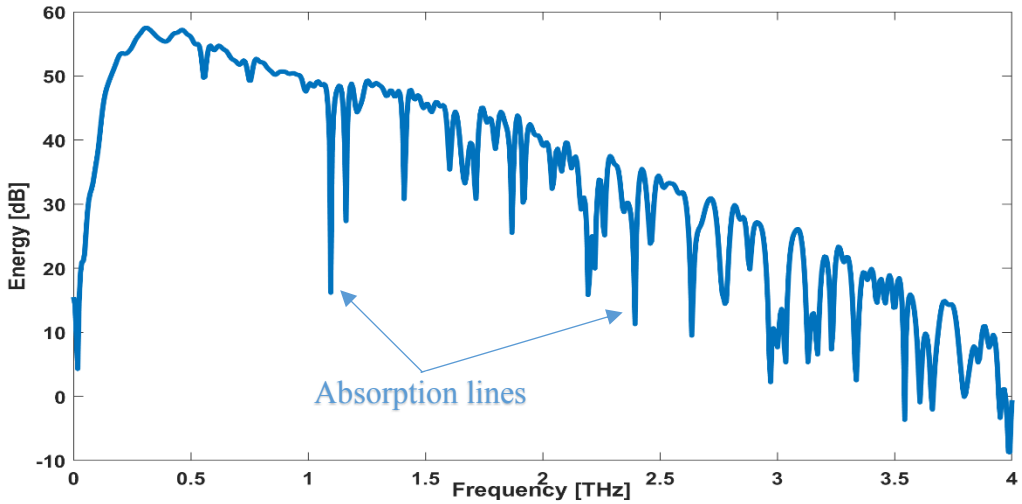

Figure 5. Pulse shape of the reference signal.

4.2 Reflection Measurement Setup

We have used several dielectric materials to conduct our measurements. These are common indoor materials found in-home or office as well as in outdoor locations. The focus is to

examine the indoor materials used as furniture for various purposes. The wavelength of the THz band is very short; thus, it highly expected to be mainly used in short distance communications. Herein, these dielectric samples have different values of permittivity. The materials used in our measurements as samples are aluminum, glass, plastic, and two different hardboard sheets in terms of width. Figure 6 shows the used samples except plastic in our measurements. Most of the samples were used to take the reflection and penetration measurements except the copper plate, which only used to carry out the diffraction measurements in particular. The other sample was plastic. Figure 6 (a) shows the thick hardboard, which used to take the reflection measurements, and the other one shown in Figure 6 (e) is comparatively thinner, which used to study the penetration properties only. The results have been discussed and analyzed in the next chapter.

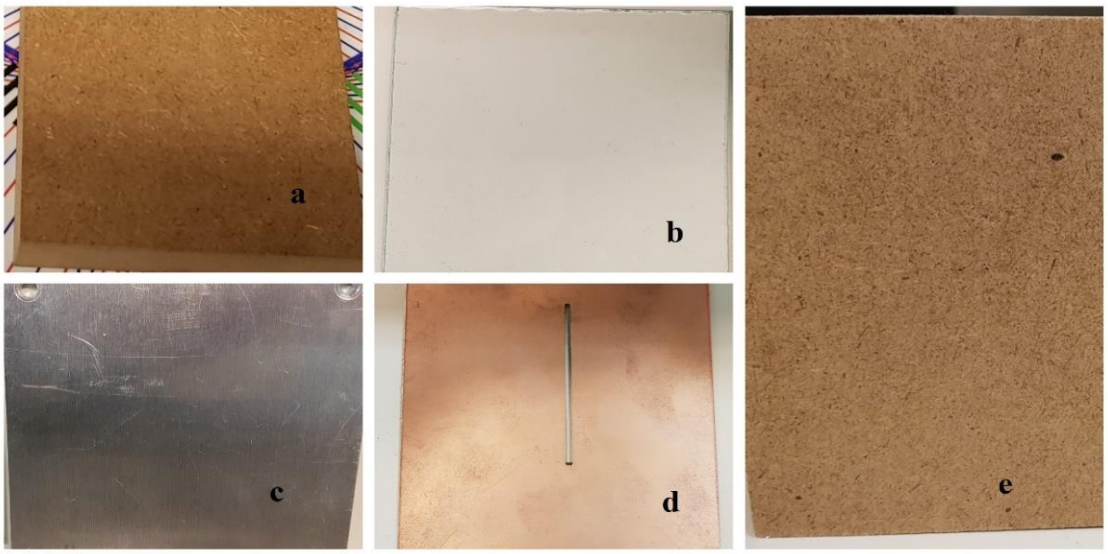

Figure 6. Used materials to conduct measurements, (a) thick hardboard, (b) glass, (c) aluminum, (d) copper plate and (e) thin hardboard sheet.

The first sample used in our measurements, aluminum, was a moderately polished sheet and smooth-surfaced. The glass sample was the smoothest sample amongst all the samples, which is typical window glass mostly found at home or office. The plastic was a styrene-acrylonitrile sheet also available in indoor locations. These two samples were almost identical in terms of width, whereas the last sample used in the experiment was the hardboard. This sample was composed of compressed wood fibers [14], and also was the roughest sample in our measurement. It mostly used as household furniture like bookshelves, tables. The materials thickness can be found in Table 1. The measurement setup with aluminum and glass samples are shown in Figures 7 and 8, respectively, at different angles. Firstly, we have taken only reflection measurements with four different samples in which two setups have been displayed here. The other two samples plastic and thick hardboard were also identically placed, likewise these figures.

The samples were placed in zero position between the Tx and Rx measurement heads. The samples were placed in such a way that the total path length remained the same for all setups, approximately 60 cm, of which 20 cm comes from the measurement plate's separation as discussed earlier and about 2×20 cm from the optics [14]. The sample was adjusted in such a way that it remains steady and 90 degree angle both in vertical and horizontal directions. We

kept the sample steady and varied the measurement heads of both Tx and Rx from 10 degree to 45 degree angle with a five degree interval.

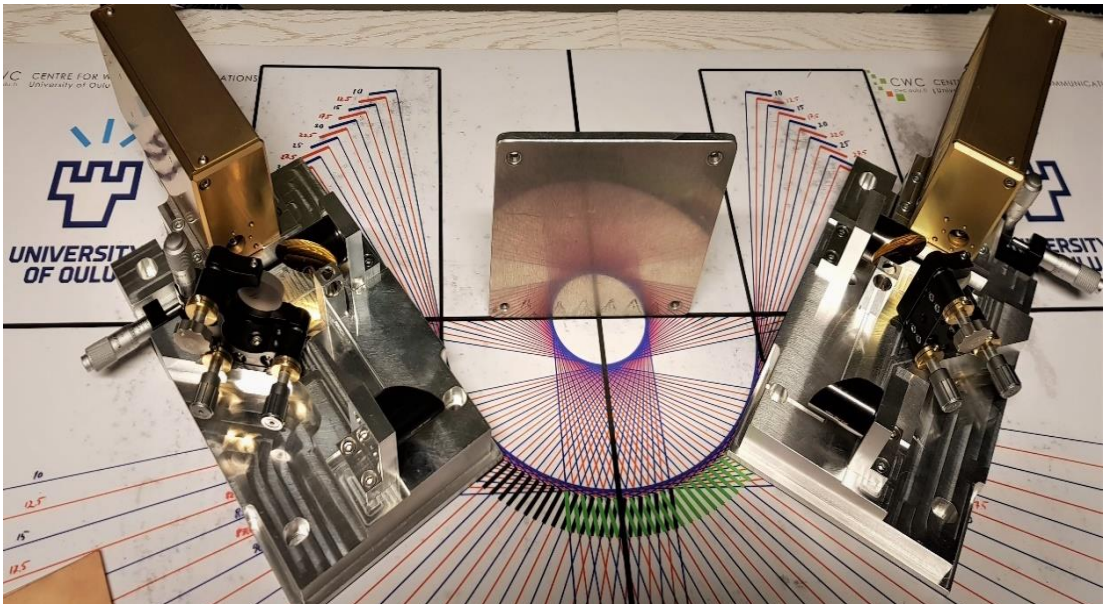

Figure 7. The measurement setup of aluminum sample when the Tx and Rx at 35 degree angle.

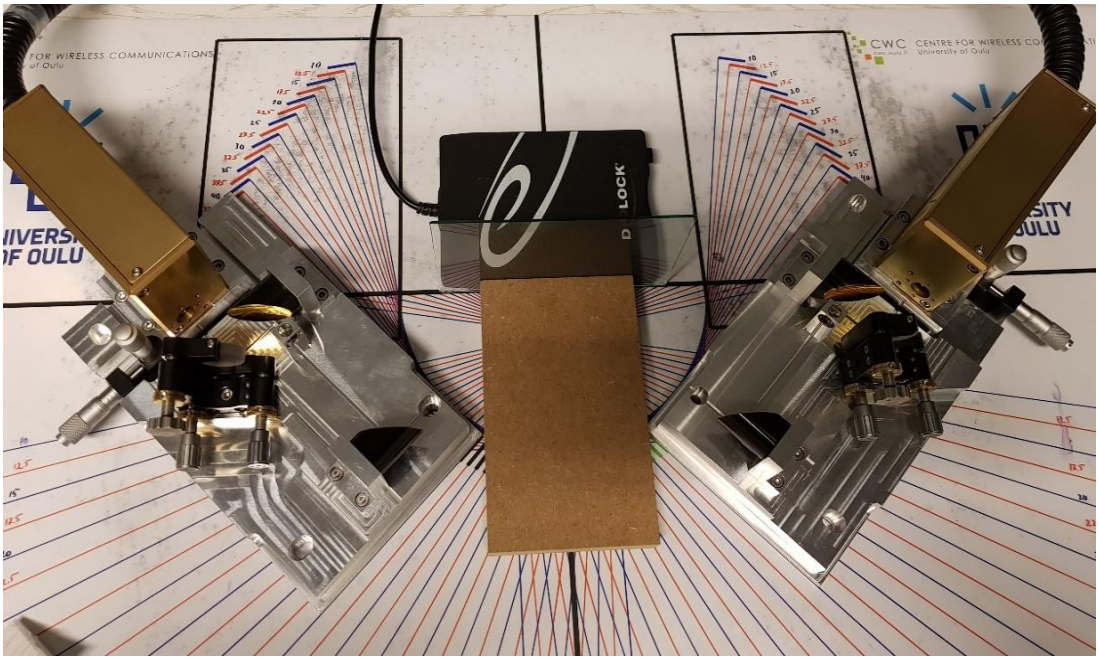

Figure 8. The measurement setup of glass sample when the Tx and Rx at 45 degree angle.

To study both reflection and penetration properties together, we formed a new multipath propagation setup with two different samples. The goal is to compare the results of this newly created multipath model with the previously discussed model. The measurement setup was the

same as earlier. However, the only difference herein was the thin hardboard was placed in front of the Tx antenna in such a way that the radiation can be incident on the material's surface orthogonally. This sample was at a zero degree angle with the Tx antenna. The objective is to analyze the behavioural changes of both the NLOS propagation model. The comparison of the measured results has been given in the next chapter.

4.3 Penetration Measurement Setup

To conduct this measurement, we have used three types of materials with different thicknesses. The measured sample thicknesses are given in Table 1. The thickness per sample is different here. The thickest among all three samples was the hardboard. The overall path length increases between the emitter and receiver with the increase of the sample thicknesses. We have placed the glass, plastic, and thin hardboard at zero degree angle in between the emitter and receiver heads in such a way that the beam can highly directed to each other. The samples were carefully placed. Thus, all samples should be 90 degrees aligned vertically and placed at a distance of 10 cm from the measurement heads.

Table 1. Measured materials thickness.

Sample	Thickness [cm]
Glass	0.16
Plastic	0.20
Hardboard	0.25

4.4 Diffraction Measurement Setup

In this setup, two types of diffractions have been reported. The common knife-edge diffraction was the main interest here. However, single slit diffraction was also studied.

4.4.1 Knife-Edge Diffraction Measurement Setup

We used a copper-plated fiber sheet to conduct the knife-edge and single slit diffractions measurement. The copper sheet has shown in Figure 6 (d). Because of copper plating, the THz radiation did not pass through the sheet. The copper-plated sheet placed between Tx and Rx at the center of the beam. The sheet placed 10 cm apart between the two antennas. The total distance from Tx to Rx was 20 cm. Thus, the distance d_1 and d_2 (Figure 2) are 10 cm for these measurement setups. Table 2 gives an overview of the parameters used to conduct these measurements. The geometry of the measurement setup presented in Figure 2. We placed the copper plate at zero degree angle between the two measurement plates. This first measurement has taken to study the perfectly shadowed region behaviour of the received signal. Then we placed the emitter plate standstill and moved the receiver from 10 to 25 degrees with a five degree interval to create diffracted path between the emitter and receiver.

Then, we created another multipath scenario to study a combination of two NLOS phenomena, e.g., penetration and diffraction. Herein, the thin hardboard sample was used as an obstacle which placed perpendicular to the signal propagation direction. The multipath model was designed in such a way that after penetration through hardboard, the THz radiation diffracted by the edge of the copper plate before received by the receiver. We put the thin hardboard before emitter to create the new multipath environment, same as the setup discussed in 4.2. It should be an identical scenario if we would choose different materials instead of thin

hardboard to study both penetration and diffraction mechanisms with this same measurement setup. The above-mentioned procedure for single knife-edge diffraction followed here to take this jointly placed samples. The receiver orientations were the same as the above procedure and varied from 10 to 25 degrees with a five degree interval. Also, the first measurement was taken at zero degree position to study the perfectly shadowed region.

Table 2. Used sample properties for both diffraction measurements.

Parameter	**Value**
Distance d_1	10 cm
Distance d_2	10 cm
Radius R	0.1 cm
Slit width a	2 mm

4.4.2 Single Slit Diffraction Measurement Setup

We have used the same copper platted sheet with a single slit screen displayed in Figure 6 (d) to conduct the single slit diffraction measurements. Here, the slit width is 2 mm. We have repeated the above knife-edge diffraction measurement procedure with this single slit screen. We have taken the first measurement at zero degree angle and then varied the angle from 10 to 25 degrees with five degrees interval. The same procedure also repeated for the jointly measured technique used to create a multipath environment to study two propagation mechanisms by making a single measurement scenario.

5 RESULTS AND ANALYSIS

This chapter includes all the measurement results with analysis and discussions. The comparison between the individually and jointly measured results have been presented. The analysis and the figures below have been obtained by using Matlab software. We compare the measured responses with a reference response, which was measured in LOS to calculate the path gains of the signal.

5.1 Penetration Loss in Frequency Domain

The pulse shapes and path gains of three dielectric materials in the frequency domain are presented in Figures 9 and 10, respectively. The materials are of glass, thin hardboard, and plastic can be visible in Figure 6 (b & e). The path gain of these three materials was calculated by using (16). These two figures are limited up to 3 THz because the noise starts to dominate the signal after 2 THz, which is clear from both figures. It is visible in the figures that the signal attenuates more with the increase of frequency, especially over 1 THz. The signal through plastic sample shows more gains than others as we get responses up to roughly 1.8 THz. The glass and hardboard both show similar responses and has lost energy significantly around 1 to 1.2 THz.

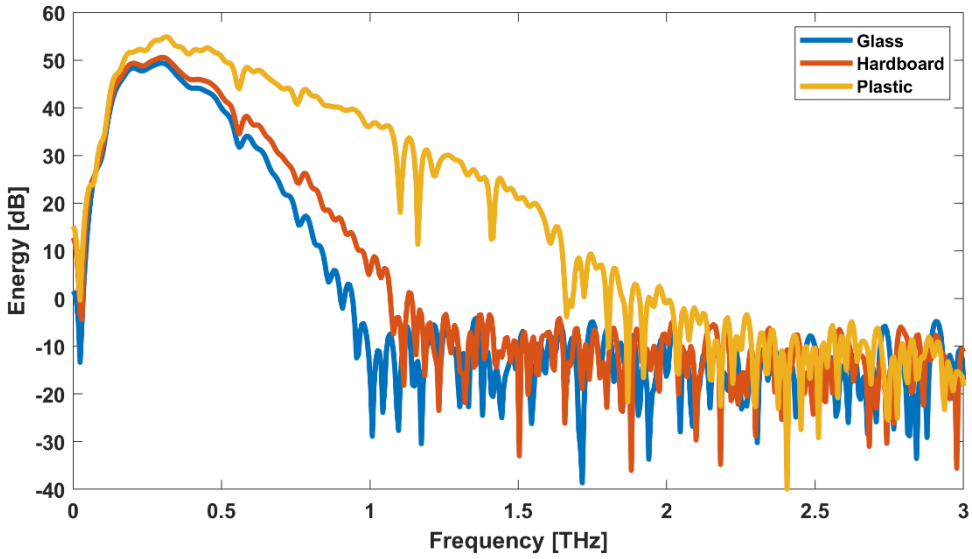

Figure 9. Pulse shapes of glass, hardboard & plastic.

In Figure 10, the path gains of these materials given in the dB scale as a function of frequency. The path gain depends on the thickness of the materials, as discussed earlier in the third chapter. We have mentioned in Section 4.3 that different thicknesses have chosen in our experiments to see the linear changes of path loss with the increase of frequency. As we can see that the penetrated path gains through these materials decreased linearly when the frequency goes higher.

The path gain through plastic shows a better response among the three samples. This material has a tolerable path loss in comparison with the other materials. Plastic allows penetration up to 1.8 THz (Figure 10),whereas glass and hardboard allow more penetration at the lower end of the THz regime. After that, the noise dominates the signal. The initial ripple in the measured

responses occurs due to the lack of accuracy of the measurement device at the lower frequencies. The measurement device is capable of measuring from 0.1 THz. So, the lower bound is 100 GHz for all the dielectric materials. The glass and hardboard show similar behavior. Glass allows penetration up to 1 THz, whereas hardboard shows a bit more up to 1.2 THz in our experiment. It can be noteworthy from the figures that the signal attenuates more when passing through the glass and hardboard in comparison with the plastic material [15], [16].

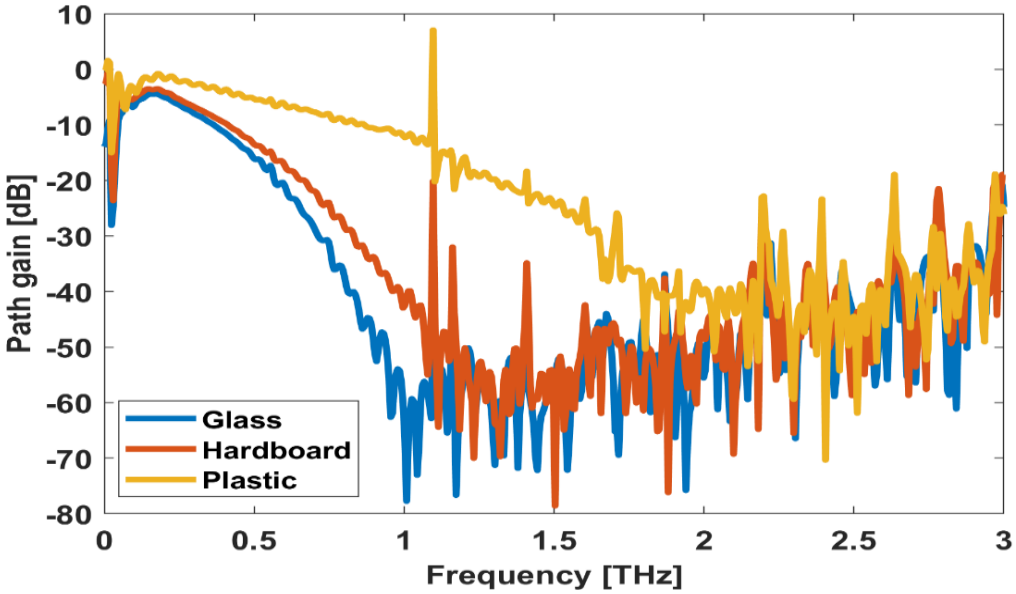

Figure 10. Measured path gains of measured samples.

The penetration coefficients of the measured samples are given in Figure 11. This figure was obtained by using (15). The signal bandwidth is dependent on the thickness of the material. If the thickness of the materials increased, then there can be seen a linear drop of the path gain in decibel-scale. The penetration coefficients can be estimated based on this information which allow to eliminate reflection loss on the material's surface [16]. The bandwidth of the penetrated signal is getting narrower, with the increase of the thickness of the materials. Thus, the signal has less energy at the higher end of the THz regime. By using penetration coefficients of those materials, we have calculated the actual loss, which is calculated by (16). This figure gives information about the penetrated signal as the reflection coefficients are valid in some frequencies where signals are not noisy [16]. The results show that the glass has a higher penetration coefficient than hardboard and plastic. This means that when the signal passes through the glass, it attenuates more than the other samples. The refraction properties of the inside of the materials is still unknown. We do not know the refraction angle when the THz signal passes those materials surface to air after penetration.

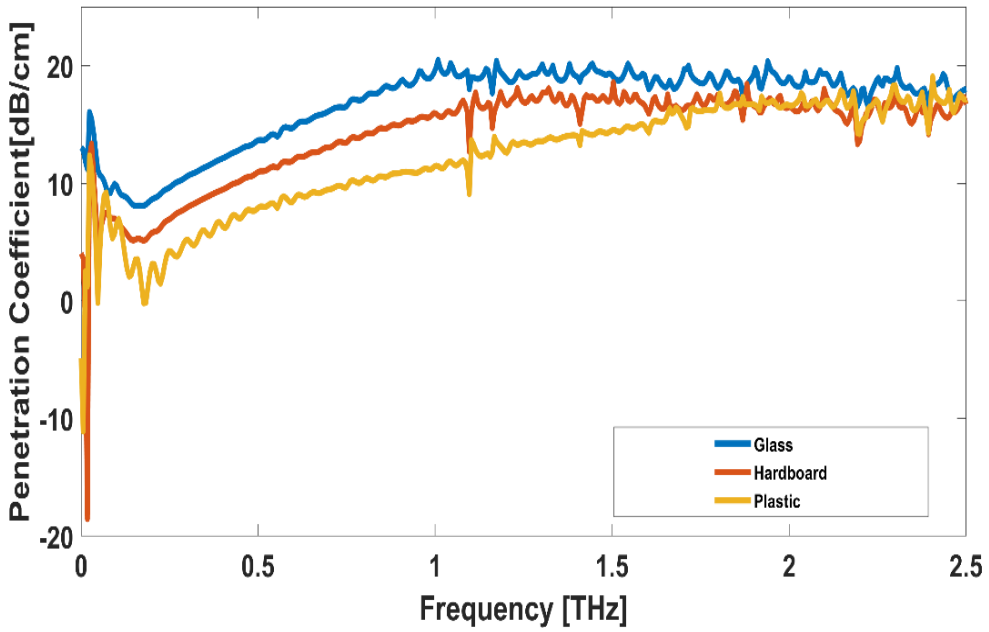

Figure 11. The penetration coefficient for the measured three samples.

5.2 Measurement Results of Reflection Properties

Figures 12 to 15, represent the path gains of aluminum, glass, plastic, and thick hardboard, respectively, at different incidence angles. The reflection angles were varied from 10 degrees to 45 degrees with a 5 degrees interval, as discussed in Section 4.2. The angle is directly relative to the tangent of the sample's surface. All figures are limited from 0.1 THz to 3 THz because the desired signal is corrupted by noise after certain level. These figures show the results of the reflection attenuation measurements of the experimented materials. The general trend is that the gain gradually decreases with the increase of reflection angles at the lower end of the terahertz band. Besides this, due to spreading loss in the THz channel, the free space path loss can also increase that causes signal attenuation [44].

In our measurements, aluminum was the strongest reflector amongst the other materials. The glass and plastic, both samples, allow penetration at some point, and while thick hardboard has absorption properties. However, aluminum does not allow penetration at all in our case. The following figure shows the results for the aluminum sample.

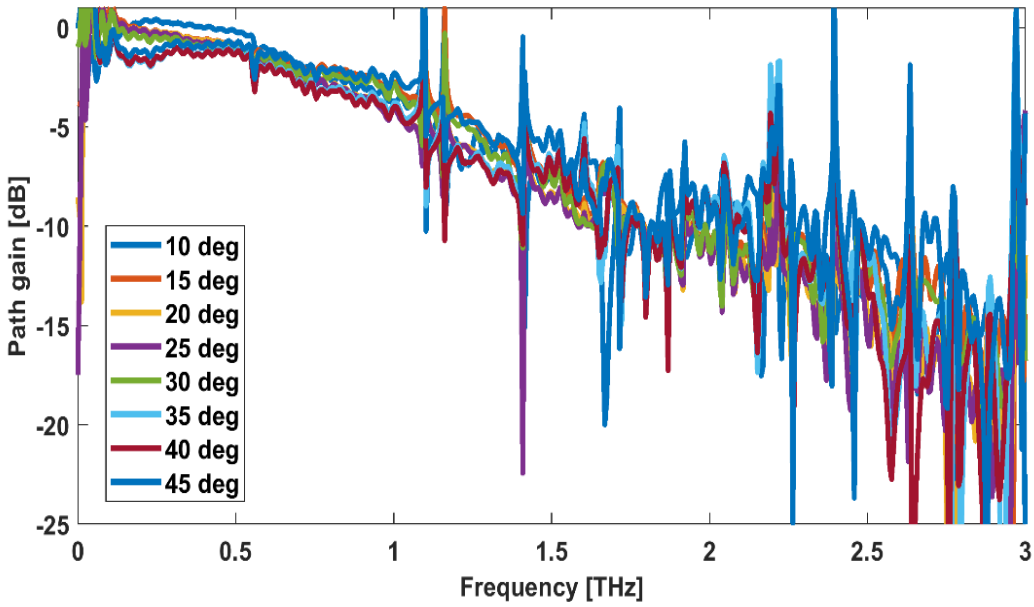

Figure 12. Path gains of individually measured sample-aluminum at different angles.

In our setup, the emitter and receiver were both in equal distance from the used materials. The highest gain obtained when the Tx and Rx both were at a 10 degree reflection angle. Figure 12 depicts that the gain is almost similar for all reflection angles in our measurement. Notably, better responses can be obtained at the lower reflections angle. The lower angles to the surface give the lowest reflection losses towards the specular directions. However, we still got responses at higher angles too. The overall trend remains the same as the lower frequency offset shows better response at higher angles than the higher frequencies at higher angles. Although, the trend differs in some cases. The disagreement can be seen at 45 degree angle that the reflected path gain is better than the reflected path gain at 40 degrees in Figure 12. This disagreement might happen due to the measurement errors which has an impact on the measurement results. Since, the Tx antenna has a highly directional beam so a slight misalignment of the samples can cause degradation of the measured responses. We were getting tolerable responses at the receiver from 2 to 2.5 THz. Aluminum, as a metal, acts as an excellent reflector in comparison with the other materials. The metal piece used during measurements was moderately polished and the surface is smooth. Therefore, it allows less scattering at the lower frequencies. Nevertheless, at higher frequencies, the smooth surface of the materials can act as a rough surface as the wavelength becomes shorter. The figure gives information about the path gain, which is around 0 to -5 dB up to 1 THz for all angles. After that, the gain declines from -10 to -15 dB between 1 and 2 THz. The sharp spikes in the figure symbolized the absorption loss was caused by molecules existing in the ambient environment when the radiation traversed through the air. Besides, when the reference signal becomes noisy then it causes spikes in figure after divisions with the measured response [14], [17], [18].

The results of the reflected path gains of glass and plastic in different angles are presented in Figures 13 and 14, respectively. The lower angle reflected path shows a better response than at the higher angles and high-frequency offset. Figure 13 shows that we can get 0 dB to around -10 dB gain under 1 THz for all the reflection angles in the case of glass. However, at that same frequency range, the plastic shows a bit lower gain as it drops from 0 dB to -15 dB.

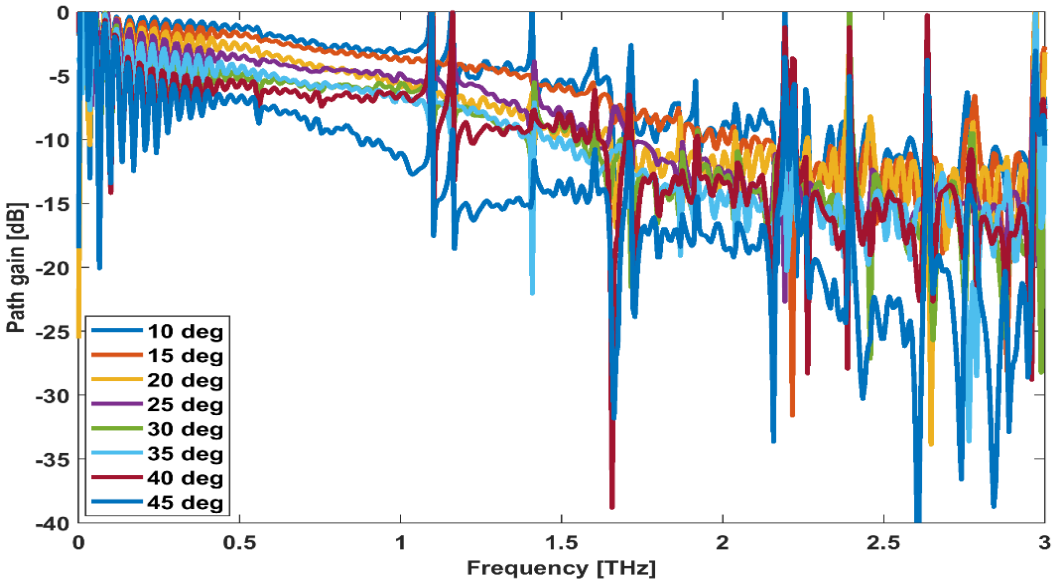

Figure 13. Path gains of individually measured sample-glass at different angles.

Nevertheless, at the higher end of the terahertz band, the reflected paths are severely limited by the molecular absorption loss. Also, the noise becomes colored by the division with the reference response. For glass, it drops around -20 dB to -30 dB when the reflection angles were more than 30 degrees and at the frequency above 1 THz. On the contrary, the plastic shows more drops in path gain above 1 THz. It dropped to around -10 dB when the angle was more than 20 degrees at 1 to 1.5 THz frequency range. These two materials also allow penetration. In the case of both glass and plastics the ripple at the lower frequencies is caused by the second reflection after penetration. This penetration loss has also affected the signal. The lower the penetration loss, the higher response can be obtained on the second reflection. Both the sample also allows scattering loss at higher frequencies as the surface is not the smoothest [14]. Signal attenuates much more because of these two losses. Despite of that, there are still responses at higher angles for both samples, but with a significant drop around -20 dB to -30 dB.

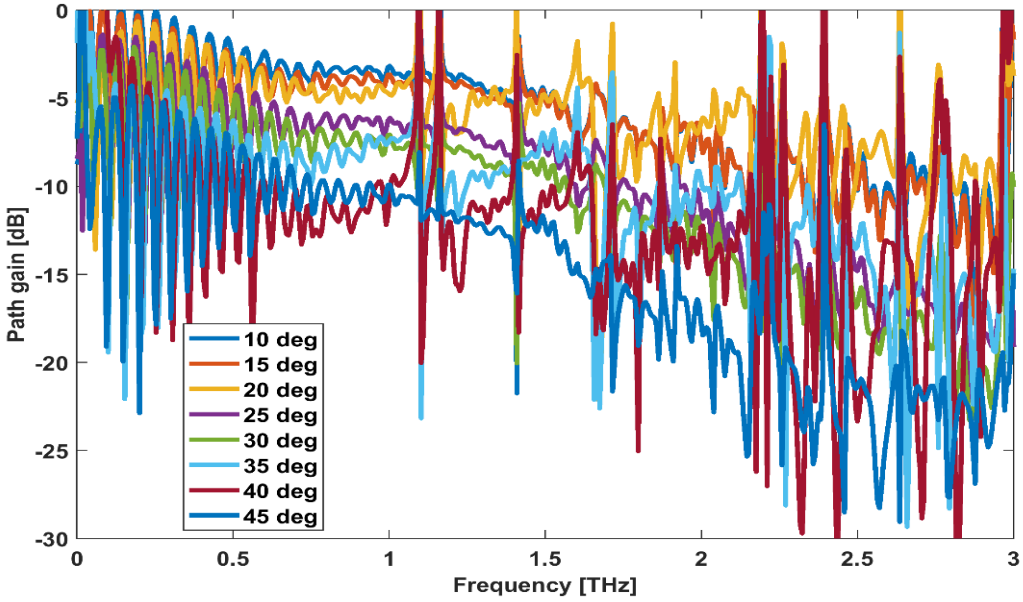

Figure 14. Path gains of individually measured sample-plastic at different angles.

After that, we have studied the reflection properties of thick hardboard in our experiment. We used comparatively thicker hardboard material for conducting reflection measurement. This sample is the roughest one amongst the four samples. Since the surface is rough, it does allow more scattering on its surface than the other three samples. For that reason, the path loss is higher than the former two materials above 1 THz. The path gain drops around -25 dB at higher reflection angles. Nevertheless, up to 1 THz, we are getting reasonable gains of around -10 dB at the higher angles. The signal attenuates more after that and goes to noise level before 2 THz. The THz signal goes below noise level in all the cases. The transmit power decreases as a function of frequency and therefore the reflection takes the signal below the noise level [14], [17], [18].

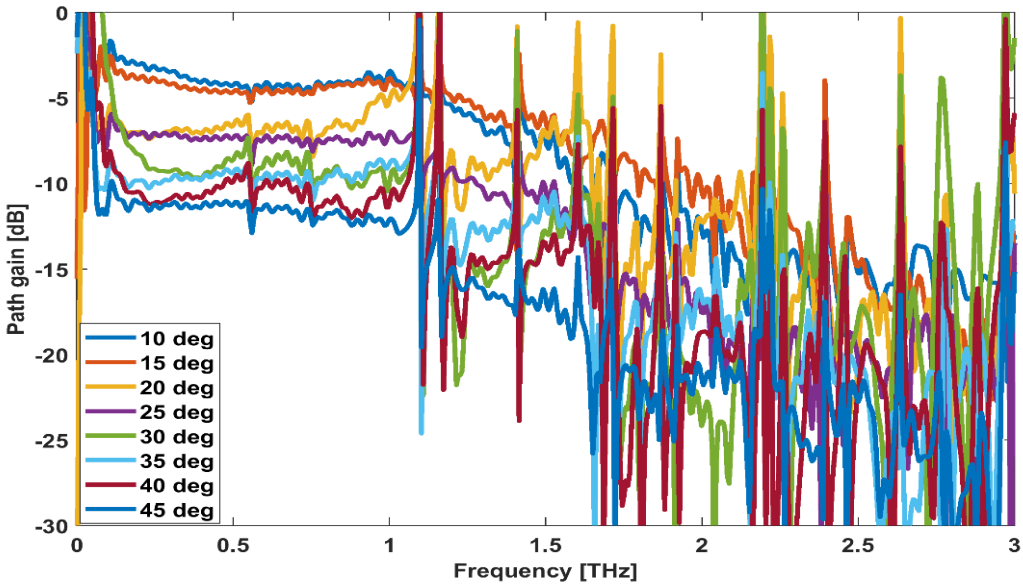

Figure 15. Path gains of individually measured sample-hardboard at different angles.

The following Figures 16 to 18 give a comparison of the reflected multipath gain of four different materials at certain angles. Figure 16 gives an interesting information that at lower angles, the glass, plastic, and hardboard show better responses in comparison with aluminum at the high-frequency offset. Since an absorption is improbable on the non-coated surface of aluminium, this might happen due to strong diffuse scattering of aluminium's surface around 1.5 THz to roughly 2 THz. Also, the refractive index might cause weaker reflections at some frequencies [14]. The reflected path gain for all the materials was almost the same at above roughly 1.2 THz. Except for aluminum, the other three materials show an almost similar gain after 0.8 THz.

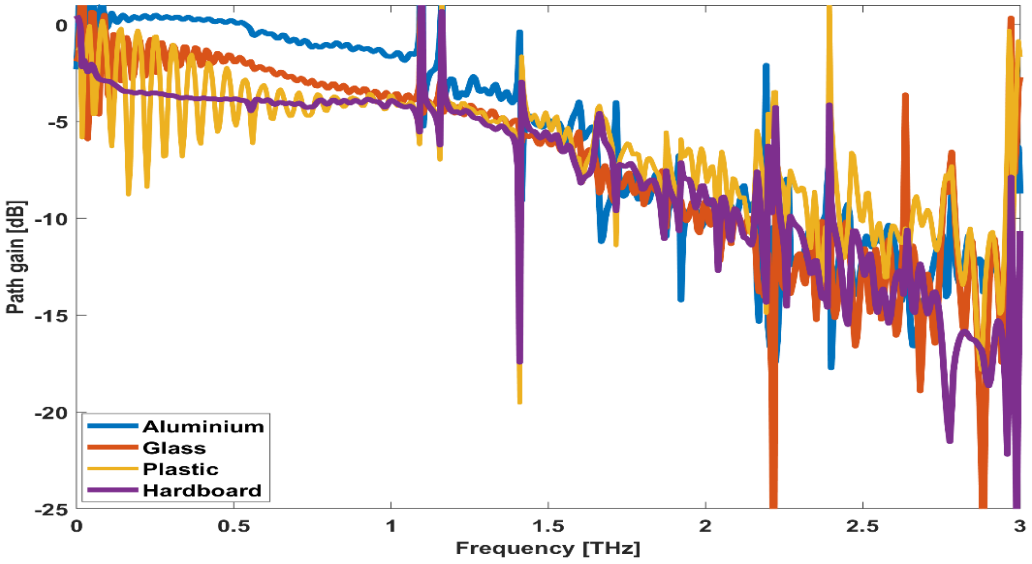

Figure 16. Path gains of the inspected materials at 15 degree angle.

Figures 17 and 18 both have a similar trend for all the materials. In Figure 17, the plastic shows almost similar gain as glass between 1.8 and 2.5 THz. At lower reflection angles, the path gain of the four samples varies around -5 dB to -10 dB when the frequency is under 1 THz. However, in higher frequency offsets such as above 1.5 THz the gain drops to around -15 dB.

From the reflection measurements we conclude that aluminum is the strongest reflector than the other three samples used in the measurements. As discussed earlier, the aluminum does not allow any penetration on its surface whether the other samples have penetration and absorption loss on their surfaces. Furthermore, the smoother surface can act like a rougher one when the wavelength gets so smaller in the high-frequency spectrum. The glass and plastic reflect the THz signal better than the hardboard. Although the general trend was the path gain drops with the increase of reflection angle, yet that is not entirely true for all cases. This variation occurs due to the misplacement of the measurement apparatus which also has an impact on the results. It also depends on the atmospheric condition of the room at a specific time [14], [17], [18].

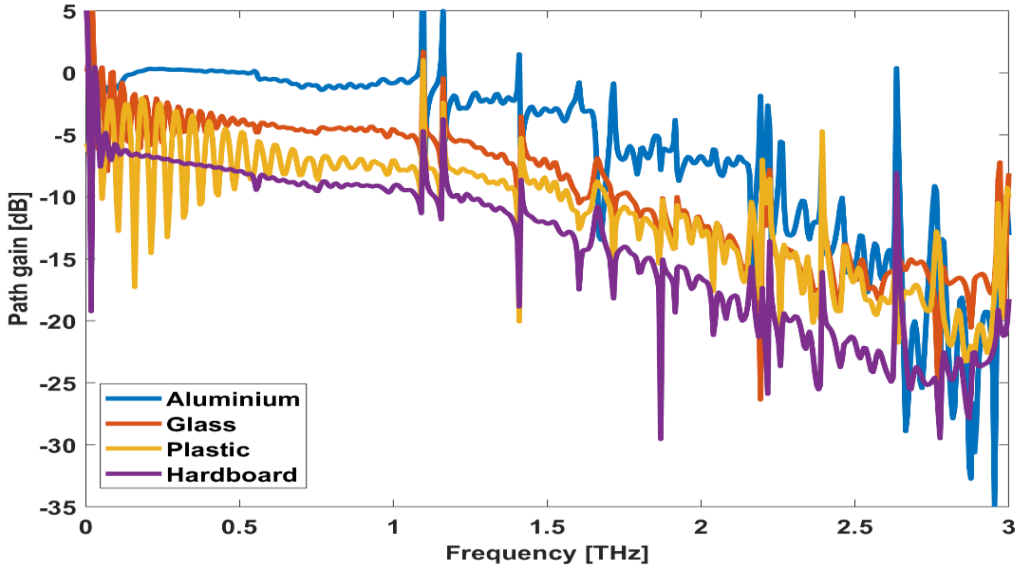

Figure 17. Path gains of the inspected materials at 30 degree angle.

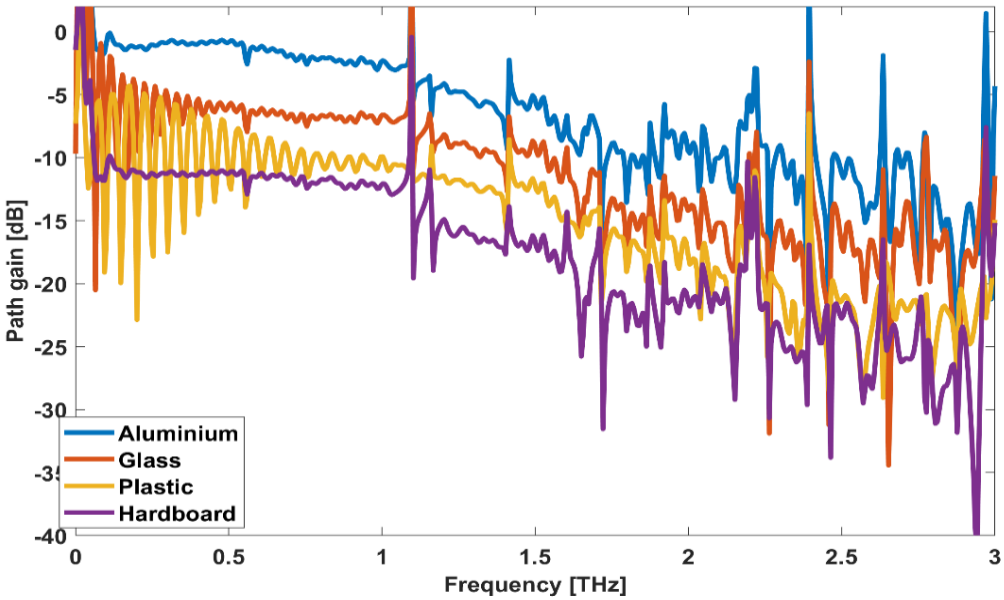

Figure 18. Path gains of the inspected materials at 45 degree angle.

5.3 Refractive Index

To model the reflection and transmission loss in the THz channel, material characterization is a necessity. As discussed in the second chapter, the reflection properties of the dielectric materials give information about the wave transmission through the materials. Refractive indices can be used to model the multipath channel modelling [19]-[20]. The list of refractive indices of the three dielectric materials used in our experiment is given in the following Table 3. It is obtained by fitting the measured reflection gains or coefficients to the Fresnel equations over the frequency band from 300 GHz to 900 GHz with an interval of 200 GHz. We find the refractive indices of glass, hardboard, and plastic at four different frequencies ranging from 300 GHz to 900 GHz with an interval of 200 GHz. We have observed the general trend of the variations of refractive index of these materials throughout the lower portion of the THz frequency band. It can be seen from the table, that the value of the refractive index is generally decreasing with the increase of frequency. Glass has the largest value amongst the three materials. Hardboard has the lowest value herein. A noticeable disagreement with the above statement is evident in the case of hardboard at 500 GHz since the value increases slightly from 1.56 to 1.60 in this case.

Table 3. Refractive index at different frequencies of the measured samples.

Materials	300 GHz	500 GHz	700 GHz	900 GHz
Glass	2.66	2.49	2.40	2.12
Hard Board (Thick)	1.56	1.60	1.55	1.40
Plastic	1.98	1.82	1.68	1.66

5.4 Measurement Results for Diffraction

The results presented in the earlier sections showed that communication through the penetrated and reflected path could be possible in the THz band. In this section, measurement results for two diffraction cases will be discussed with corresponding theoretical results.

5.4.1 Knife-Edge Effect

The most frequent diffraction phenomena that occur in the communication channel is the knife-edge diffraction of the electromagnetic wave. Figure 19 shows the result of the theoretical knife-edge effect in dB, which is obtained by (28). The parameters used in our experiment are given in Table 2 and discussed in Section 3.8. The measured knife-edge path gains in dB presented in Figure 19 as a function of frequency and diffraction angle. Both the figures were plotted from 0.1 THz to 2 THz. The measurement device is functioned to measure from approximately 0.1 THz to 4 THz frequency. Because of the pulse shape (Figure 5), the frequency bands under 100 GHz are not useable. The theoretical and measured values of both figures are suppressed to give the minimum path gain of -70 dB. We compare the measurement results with the reference signal, which was taken in LOS channels. The theoretical and the measured effect shows results up to 25 degrees diffraction angles [21].

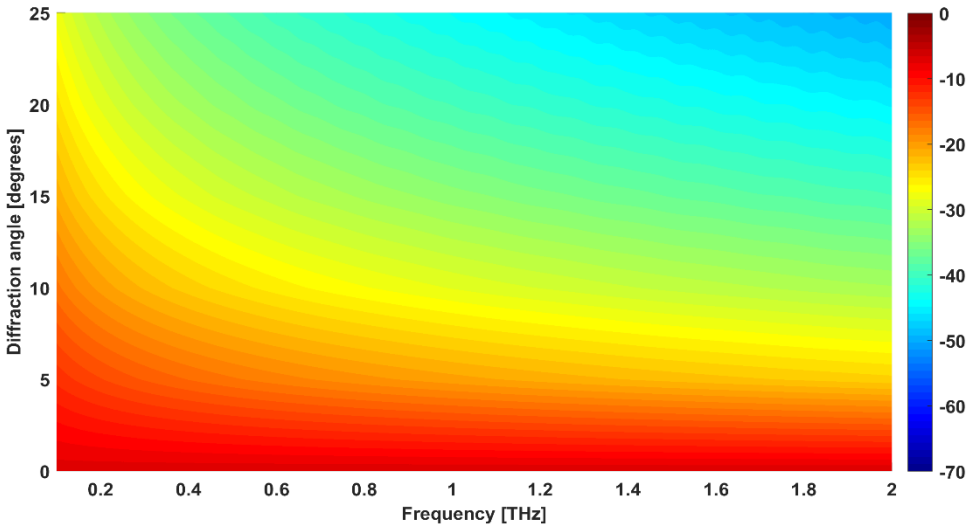

Figure 19. Theoretical knife-edge effect.

The setup was mentioned in the previous chapter, and the measurements were taken by varying the receiver from 0 to 25 degree angles. The measurement taken at zero degree angle was to study the transmission in the shadowed region of THz radiation. It gives a very good response as it not entirely affected by the multipath fading, which is the crucial phenomenon to deal with in THz band communication. Figure 20 shows the measured knife-edge response as a function of frequency and diffraction angle. The measurement result has shown a good match with the theoretical knife-edge effect result. The above plot gives an idea about how the gain decreases with the increase of frequencies and diffraction angles. At higher frequencies, the path gain drops rapidly to the noise level with the varying diffraction angles. Herein, the drop varies from 0 dB to -10 dB at the lower diffraction angles. It is noteworthy that up to 10 degree angle, the diffracted path gain is quite reasonable for all the frequencies. When the diffraction angle goes higher or 10 to 15 degrees, we get tolerable responses up to 0.6 THz. However, when the angle goes to the 25 degree angle, we can see from the plot that we can get signal responses up to 1.1 THz. After that, the noise dominates the signal. From 15 degree to higher angles, the signal affected by the noise and signal attenuation exponentially increases after 1 THz. The blue marks indicate the absorption loss in the air, which looks sharp after 1 THz and higher angles [21].

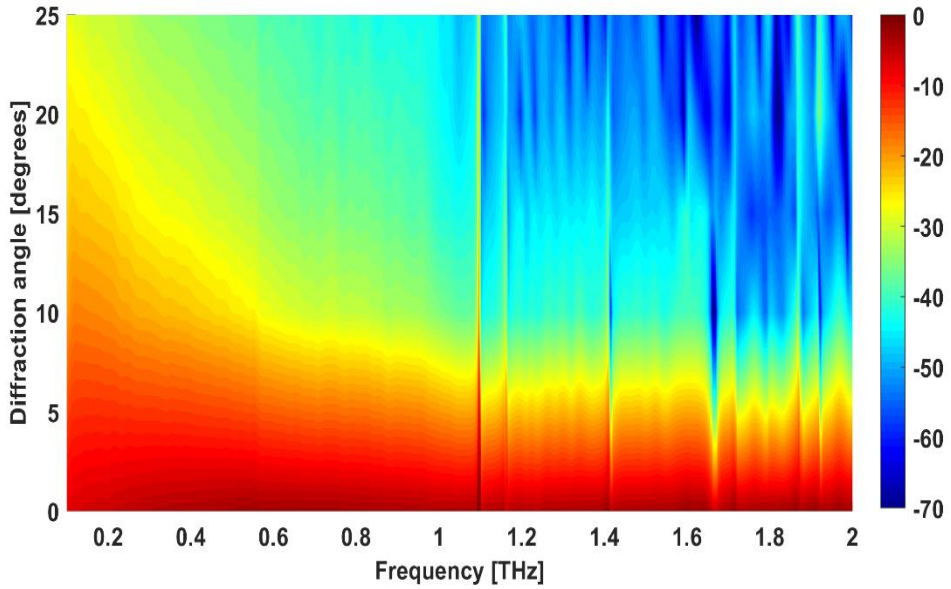

Figure 20. Measured knife-edge effect.

The pulse shape of the measured knife-edge diffracted path can be seen in Figure 21 as a function of the energy and frequency. The diffracted path at zero degree angle is indicating that the radiation intensity is quite high over frequencies. Since, it has partial LOS path. The THz signal travels in the shadowed region of the obstacles. The diffraction decreases with the increase of frequencies. The response is getting weaker with the increase of diffraction angles as well.

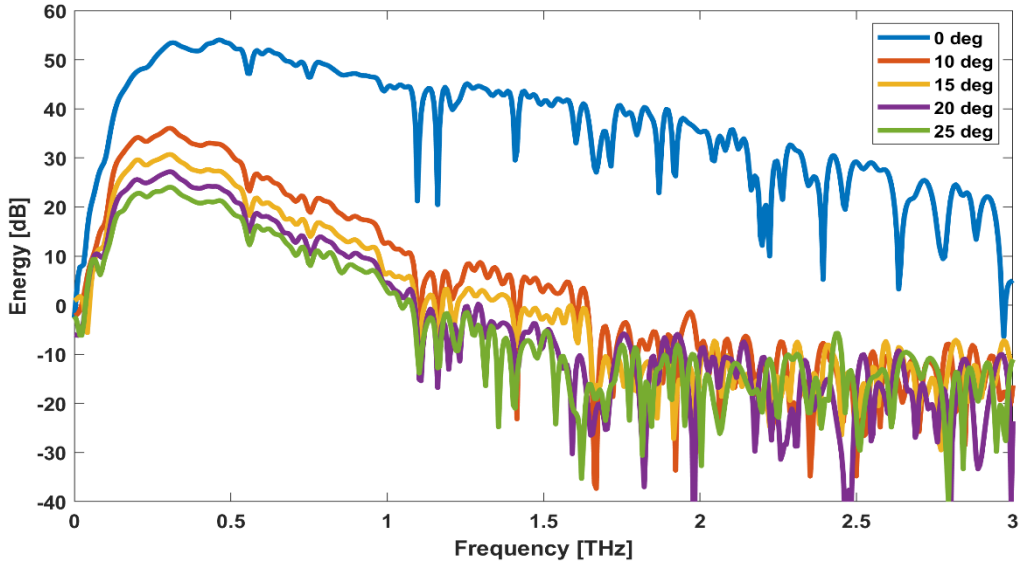

Figure 21. Pulse shapes of measured knife edge effect.

5.4.2 Single Slit Effect

Figure 22 shows the theoretical single slit effect as a function of frequency and diffraction angle in degrees. It is obtained by (29). Both the theoretical and measured figures are restricted to a path gain of -50 dB. The diffraction angles were varied from 0 degrees to 25 degrees, similar

to knife-edge measurement. At zero degrees, the path gain was high because the signal propagates directly in the shadowed region. The measured single slit path gain presented in Figure 23. This figure was obtained by comparing the reference signal with the measured responses. The measurement data is becoming noisy at higher frequencies after 1 THz. However, when the angle increases, path gain decreases exponentially. At the higher frequencies, the gain is reduced to noise level with the increase of the diffraction angles. The path gain is around -15 dB to -20 dB at lower angles up to 0.1 THz. After that, the path gain drops to around -25 dB to -30 dB above one terahertz frequency offset. The figure shows blurry results because of the diameter of the beam.

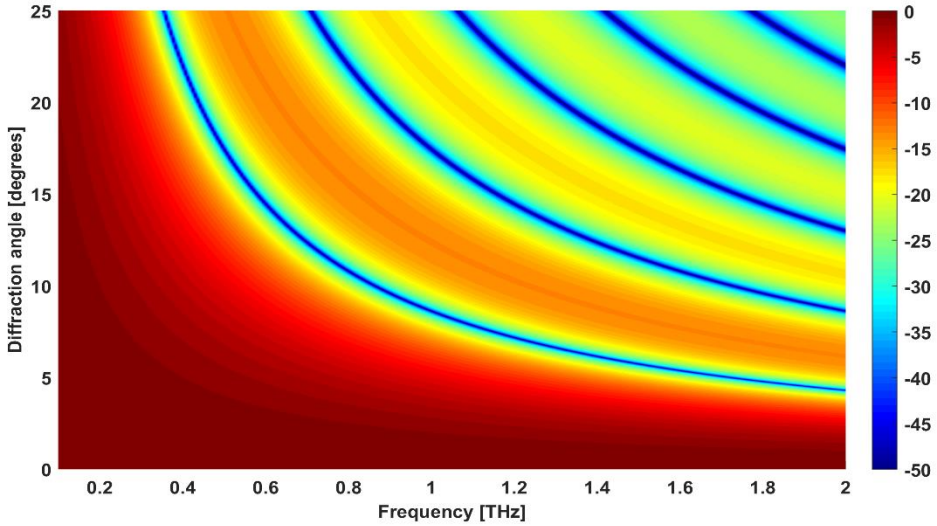

Figure 22. Theoretical single slit effect.

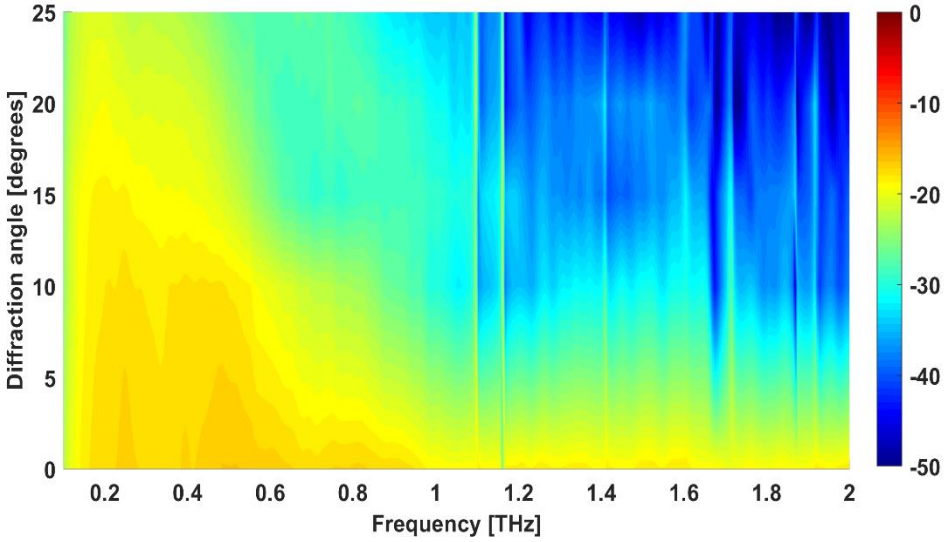

Figure 23. Measured single slit effect.

The pulse shape of the measured single slit effect showed in Figure 24 as a function of energy and frequency. The response is getting weaker with the increase of diffraction angle like the

knife-edge effect. Herein, the strongest measured response is at zero degree angle since it has partial LOS path.

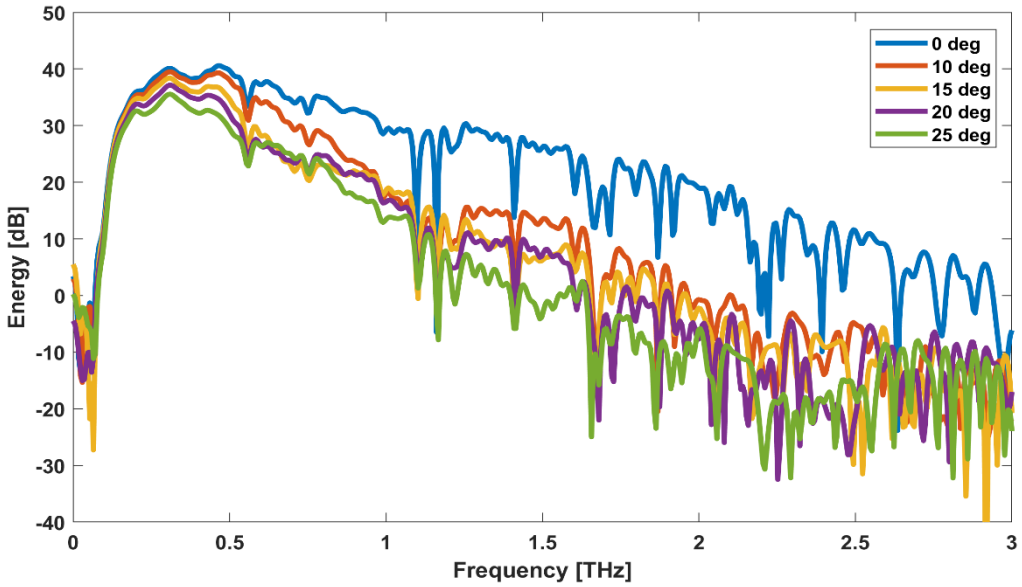

Figure 24. Pulse shapes of measured single slit effect.

5.5 Jointly Measured Results

The jointly measured techniques were discussed in the fourth chapter. The main prospects of this measurement scenario are to design a multipath NLOS propagation model that can measure the total multipath gain after the terahertz wave encounters at least two propagation phenomena. We created the multipath scenario (penetration => reflection; penetration => diffraction) where the wave first penetrated through a dielectric material and then encountered another obstacle. Later either reflected or diffracted from or by that obstacle before received at the receiver. We used the term "jointly measured" to refer to this measurement scenario. Such a measurement setup consists of two samples for each measurement. The thin hardboard was used in all measurement setup for including penetration component in the results. These samples can be visible in Figure 6(e). Earlier in this thesis, we showed the results of the single NLOS model for several samples. We measured the multipath gain by designing single phenomena like reflection, diffraction, and penetration for individual samples. Here, we are trying to measure at least a combination of two NLOS phenomena. Following that, we compare the jointly measured gain with the individually taken measured gain discussed in the previous sections for the validation of our work.

5.5.1 Joint Penetration and Reflection Loss

Figure 25, displays the reflected multipath path gains of the jointly measured materials aluminum and thin hardboard at different angles. The measurement setup was discussed in Section 4.2. In Figure 25, the result shows that the signal attenuated rapidly above one terahertz when aluminum used as a reflector. The path gain is obtained by comparing the measured response with a reference signal. The path gain is notably lower at the higher frequencies. The attenuation is very high, and signals entirely dominated by the noise above 1.2 THz. As the

signal experiences penetration loss and multiple reflection losses before reaching the receiver. There is an additional delay added to the signal.

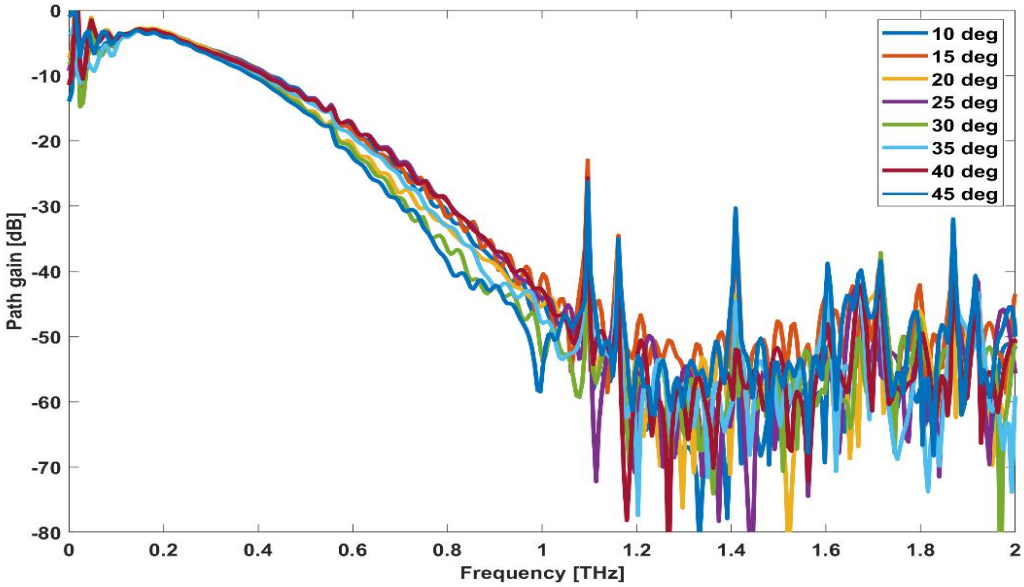

Figure 25. Path gains of jointly measured (aluminum & thin hardboard) samples at different angles.

However, aluminum still acts as a good reflector for all reflection angles. The hardboard was placed at a zero degree position in front of the emitter. Thus, the radiation, incident orthogonally on the surface of the hardboard. The overall multipath gain at the receiver drops 0 dB to -10 dB at 0.2 THz and path gain drops substantially over -40 dB around 1 THz. After 1.2 THz, the noise completely dominates the signal [14].

We compare the results of individually taken measurements discussed in Section 5.1 and 5.2, respectively, with the jointly measured results are presented in Figures 26 to 28 at three different angles when aluminum sample used as a reflector in the measurement. The term "Individually measured," used in the plot is the calculated path gain of the two separately taken measurements. The separately taken path gains have been multiplied to obtain the total gain values for the individually measured samples. This jointly measured result is the penetrated path gains through hardboard and reflected path gain of four different samples discussed in Section 5.2. The overall results are identical at every other angle. Thus, the results for three different angles have been presented here. These results show a good match between the two separately taken measurements.

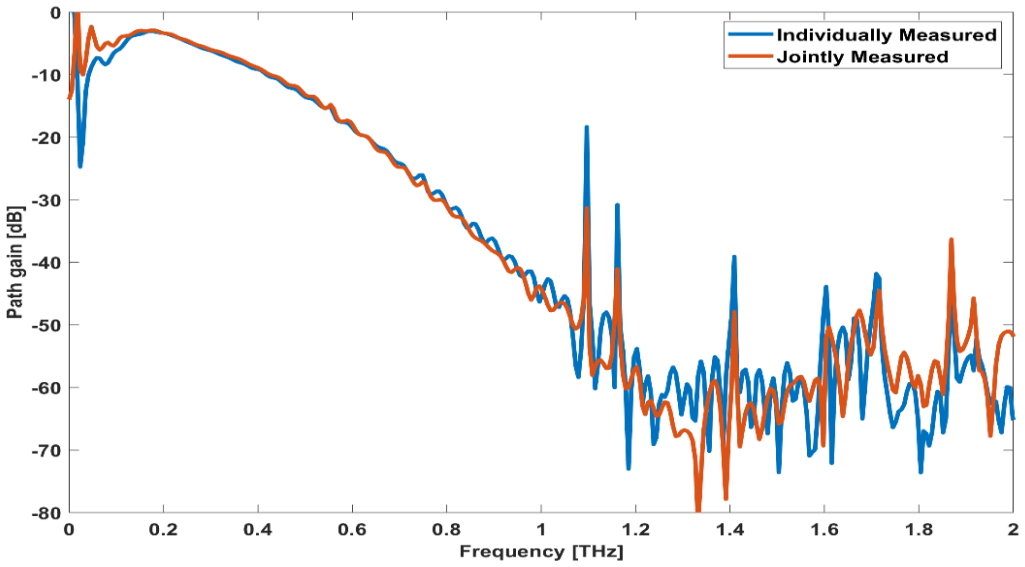

Figure 26. Comparison of individually and jointly measured path gains at 10 degree angle when aluminum was used as reflector.

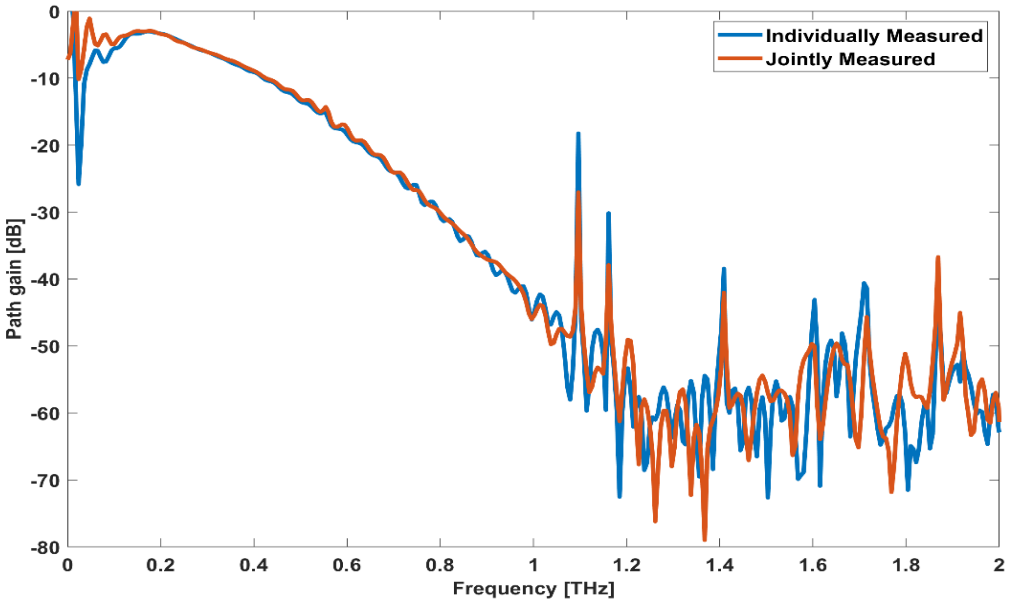

Figure 27. Comparison of individually and jointly measured path gains at 30 degree angle when aluminum was used as reflector.

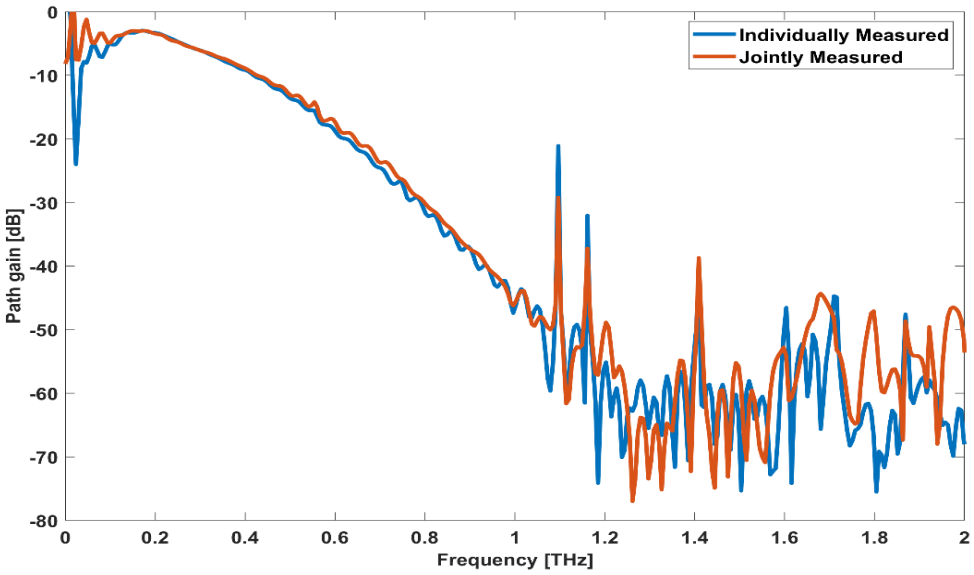

Figure 28. Comparison of individually and jointly measured path gains at 45 degree angle when aluminum was used as reflector.

The following Figure 29 displays the multipath gain for the jointly measured samples when the glass used as a reflector. The path gain varies around -10 dB to -20 dB at 0.5 THz for all the reflection angles. The signal started to become attenuated drastically at around 0.8 THz. The signal response goes under the noise level completely at around 1 THz. The results up to 2 THz have been presented here. There is linear path loss with the increase of the reflection angles and frequency.

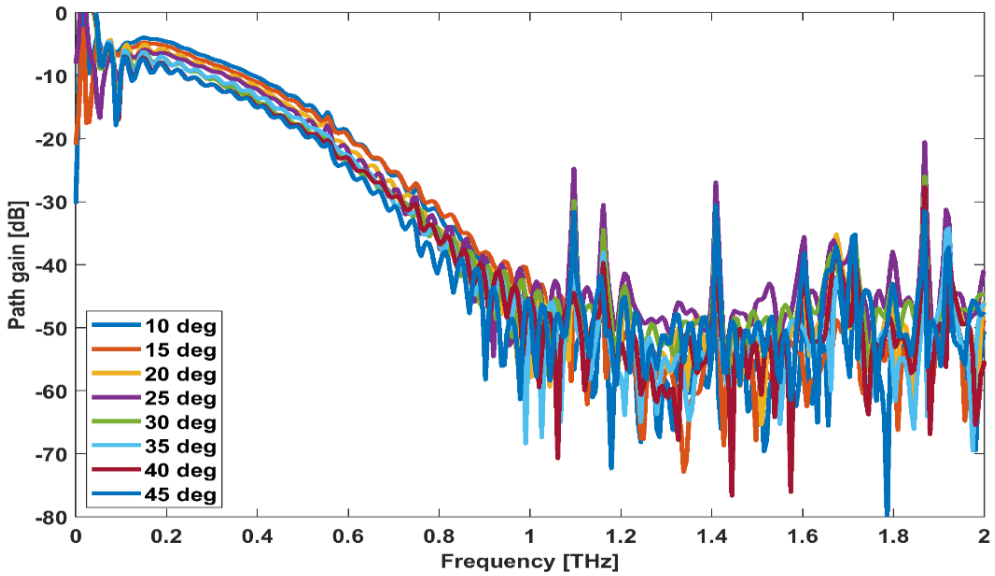

Figure 29. Path gains of jointly measured samples (glass & thin hardboard) at different angles.

As discussed in Section 5.1, the thin hardboard almost filtered out the high-frequency component. We get the final multipath gain, which is later reflected by glass. Figures 30 and

31 show the comparison of the two multipath measurement results at 10 and 40 degrees, respectively, when glass used as a reflector. At 10 degree angle, the path gain is almost similar in both cases. The path gain varies from -5 dB to -20 dB at around 0.4 to 0.6 THz. After that, the path loss is very significant. In Figure 31, the individually measured path gain, which is the multiplication of individually reflected and penetrated paths, shows better gain at some frequencies. However, the considerable path gains up to -20 dB can be obtained up to 0.5 THz at a higher angle also. The path gain was -40 to -50 dB at around 1 THz when Tx and Rx were placed at a 10 degree reflection angle. But at 45 degree angle, the pathloss is significantly high. The two measured responses are very well matched in lower angles, but slight deflection occurs at 45 degree angle.

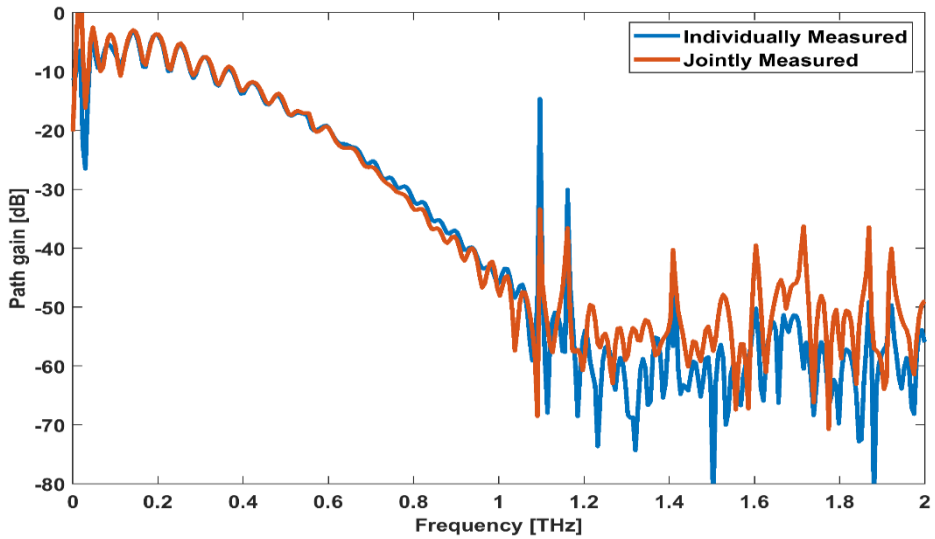

Figure 30. Comparison of individually and jointly measured path gains at 10 degree angle when glass was used as reflector.

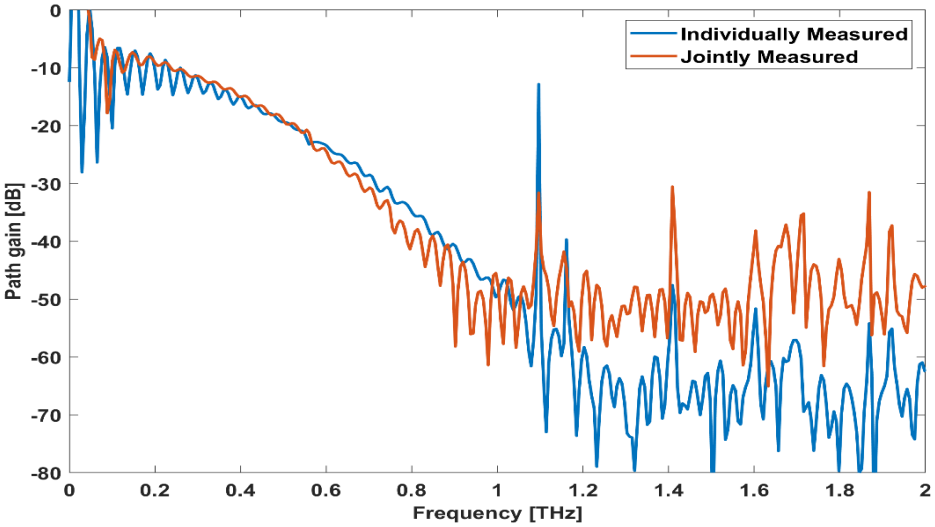

Figure 31. Comparison of individually and jointly measured path gains at 45 degree angle when glass was used as reflector.

The results of plastic used as reflector are presented in the following Figure 32. The plastic shows a comparatively lesser path gain than the glass. The path gain is not smoother in comparison to the results of the previous samples. The path gain varied from 0 dB to -20 dB at around 0.3 to 0.4 THz, which is somewhat considerable. However, the gain drops to -30 dB and higher after 0.5 THz onwards. The noise dominates the results after 0.8 THz in this case. The comparison between the individually measured results and jointly taken measurement results are presented in Figures 33 and 34, respectively. The two results match very well.

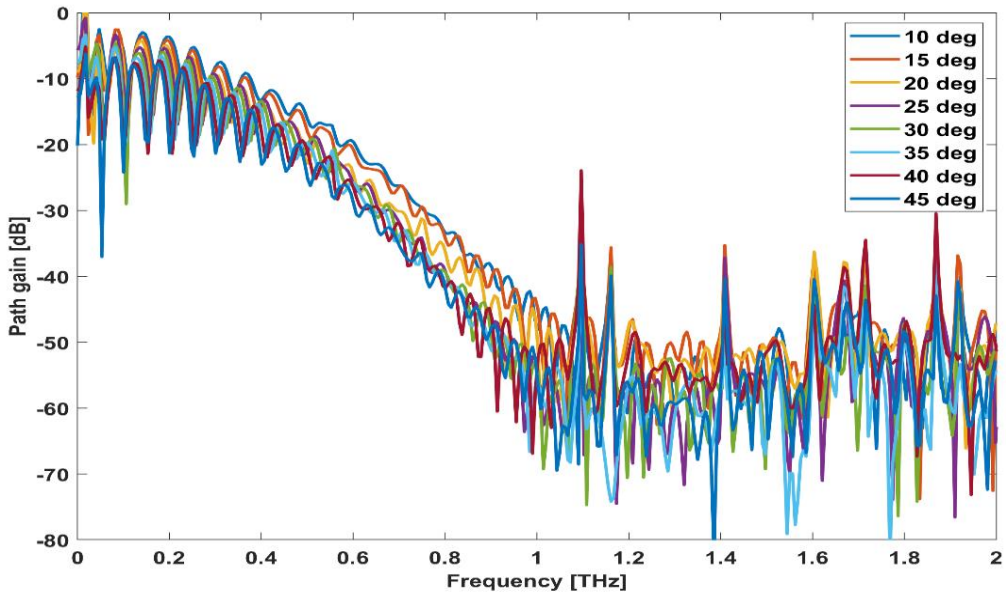

Figure 32. Path gains of jointly measured samples (plastic & thin hardboard) at different angles.

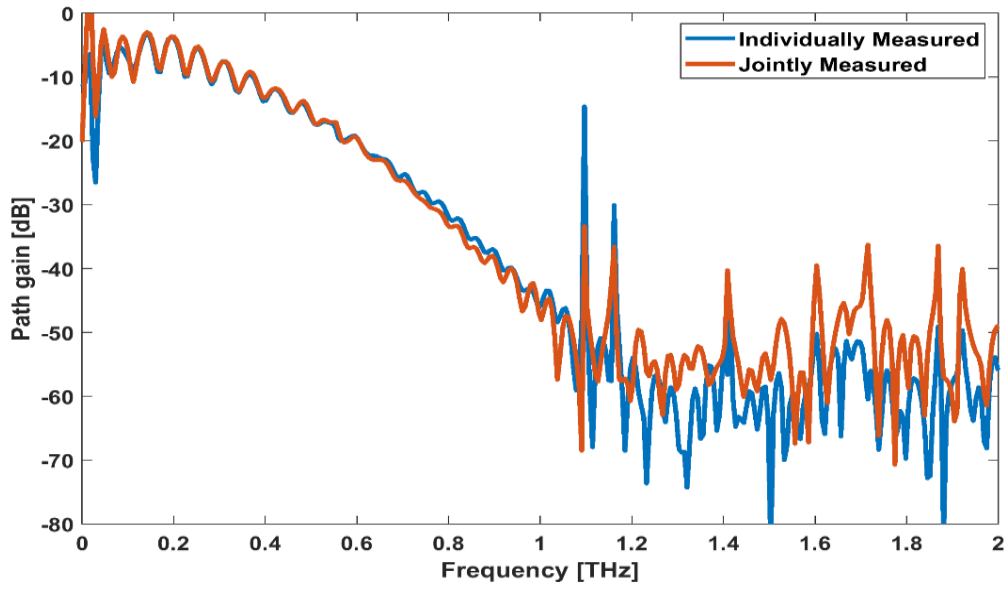

Figure 33. Comparison of individually and jointly measured path gains at 10 degree angle when plastic was used as reflector.

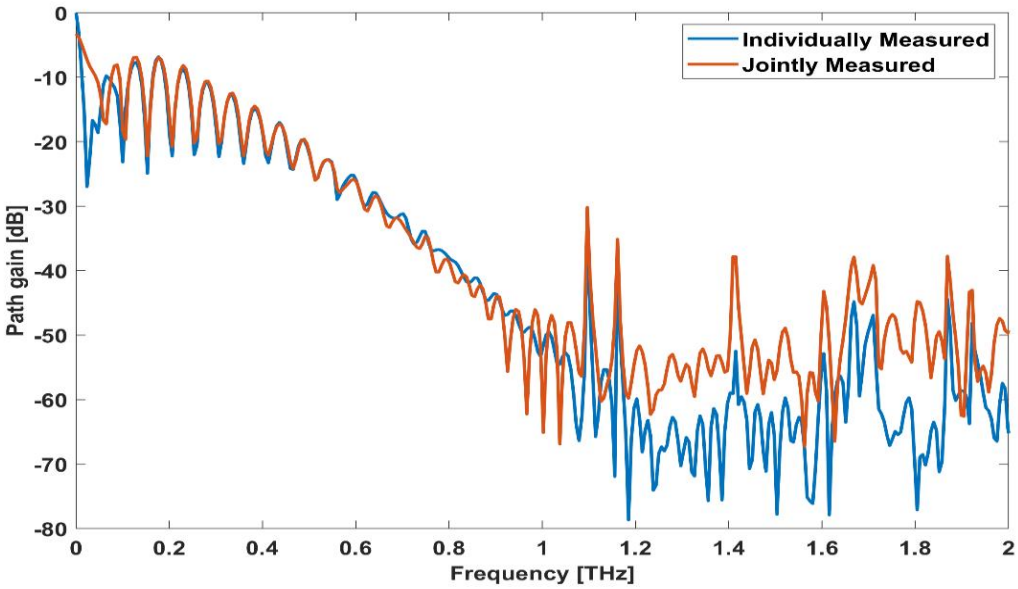

Figure 34. Comparison of individually and jointly measured path gains at 40 degree angle when plastic was used as reflector.

The results of jointly measured penetration and reflection loss of two hardboard materials displayed in the following Figure 35. Here, the thick hardboard was used as a reflector. The figure shows that the path gains linearly dropped with the increase of reflection angles. The interesting point in this figure is that the multipath gain at the 35 degree angle shows a better response than the path of the 30 degree angle. However, the general trend remains the same as path gain decreases with the increase of reflection angles. Hardboard act as a better reflector at some frequency spectrum, even in higher angles. Hence, sustainable path gain can be obtained up to 0.5 THz. The path gain drops drastically from near about -50 dB to -60 dB at 1 THz frequency.

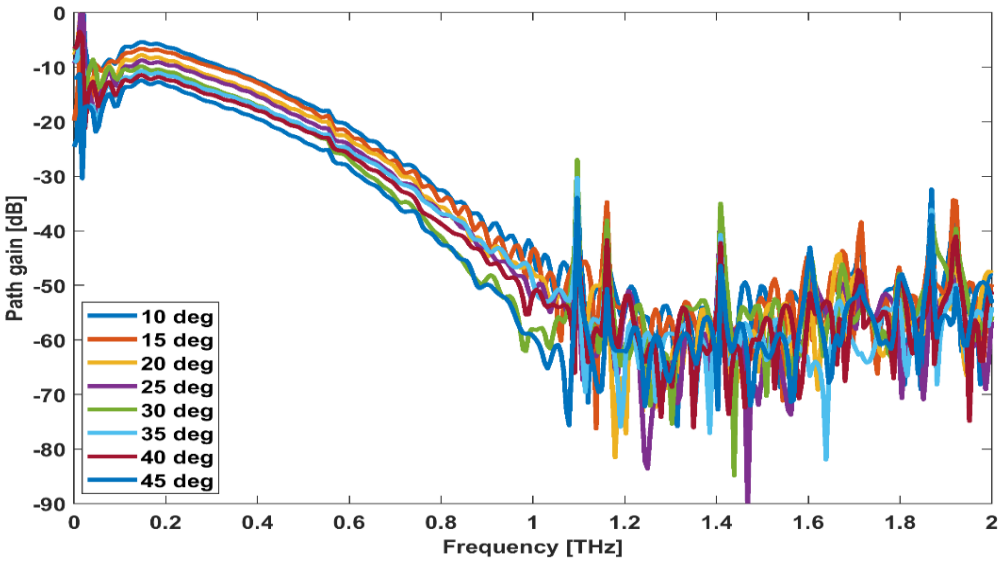

Figure 35. Path gains of jointly measured samples (thick hardboard & thin hardboard) at different angles.

The following two Figures 36 and 37 represent the comparison at the 10 degree and 30 degree reflection angle respectively. At a low angle, the results show a slight deviation as individually measured multipath has shown better gain above 0.5 THz frequency. Nevertheless, the latter figure exhibits a well matching plot before the signal becomes entirely noisy. It can be observed that for every above plot, the noise dominates after 1 THz of frequency in terms when two NLOS phenomena occur in the THz wireless channel.

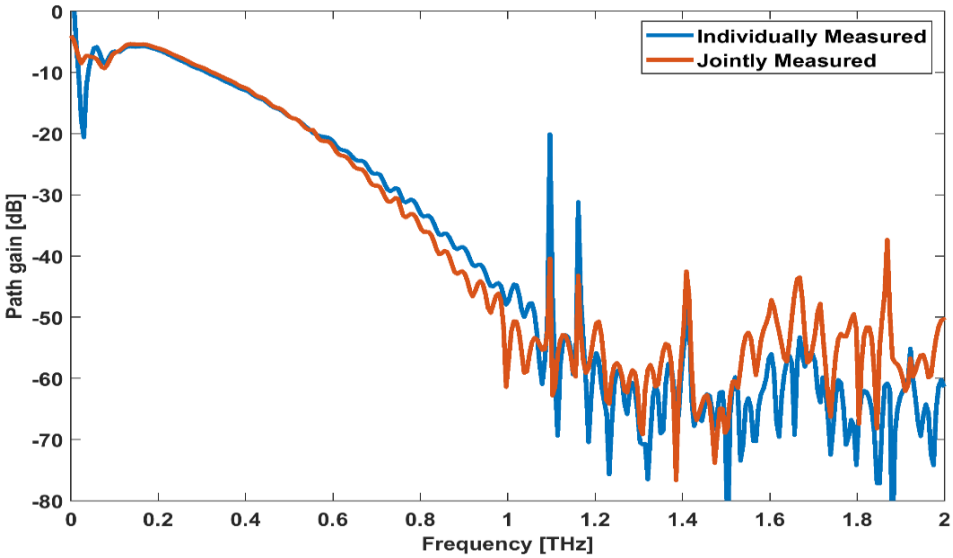

Figure 36. Comparison of individually and jointly measured path gains at 10 degree angle when thick hardboard was used as reflector.

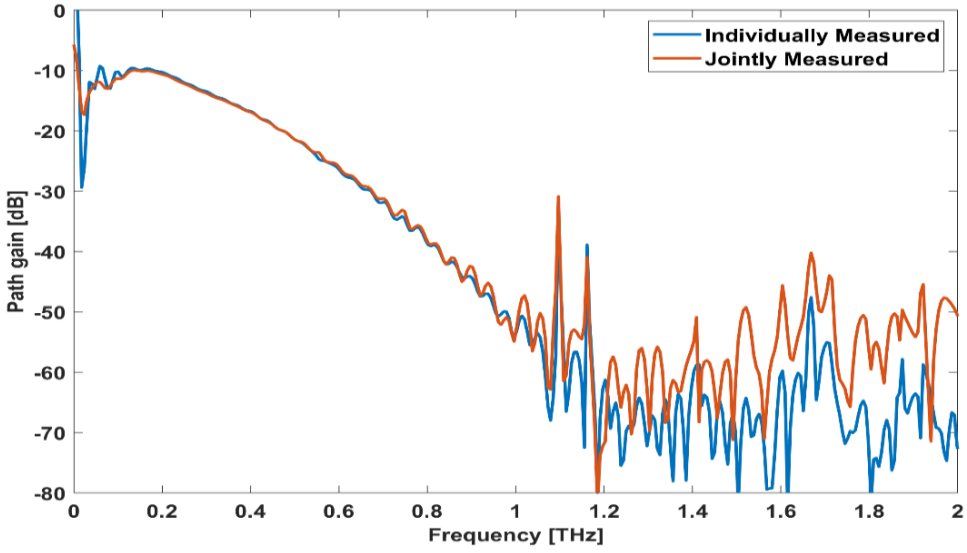

Figure 37. Comparison of individually and jointly measured path gains at 30 degree angle when thick hardboard was used as reflector.

5.5.2 Joint Penetration and Diffraction Loss

The combination of two NLOS phenomena such as penetration and diffraction measurement results will be presented in this section. The measurement technique for joint penetration and diffraction has been discussed in Section 4.4.

5.5.2.1 Knife-Edge Effect

Figure 38 shows the visual presentations of the measured response as a function of frequency and diffraction angles. This figure was obtained by dividing the reference response taken in full LOS condition. The right-side color bar indicates the signal intensity of the measured responses. The results are displayed from 0.1 THz to 2 THz. The calculated knife-edge response was obtained by the multiplication of two single NLOS phenomena discussed in Section 5.1 and 5.4.1. Figure 39, represents the calculated knife-edge effect. We calculated the total multipath gain using Matlab and plotted visually to show the comparison of the total path gain of two distinct scenarios. The jointly measured effect looks a bit blurry at higher frequencies and higher diffraction angle than the combined multipath effect. However, the path gain is almost similar under 1 THz frequency. The path gain drops exponentially with the increase of diffraction angles for both cases. The multipath fading occurs in the channel affects the signal responses significantly. From the figure, it can be seen that up to 15 degree angles, the path gains vary from 0 dB to -20 dB approximately, under 0.8 THz.

We still get responses at 0.7 GHz when the receiver was at a 25 degree angle with the transmitter. However, the path loss is very high. The noise part seized the main information after 0.7 THz at higher angles and around 1 THz at lower angles, respectively. In both cases, the considerable path gain can be obtained only at lower angles.

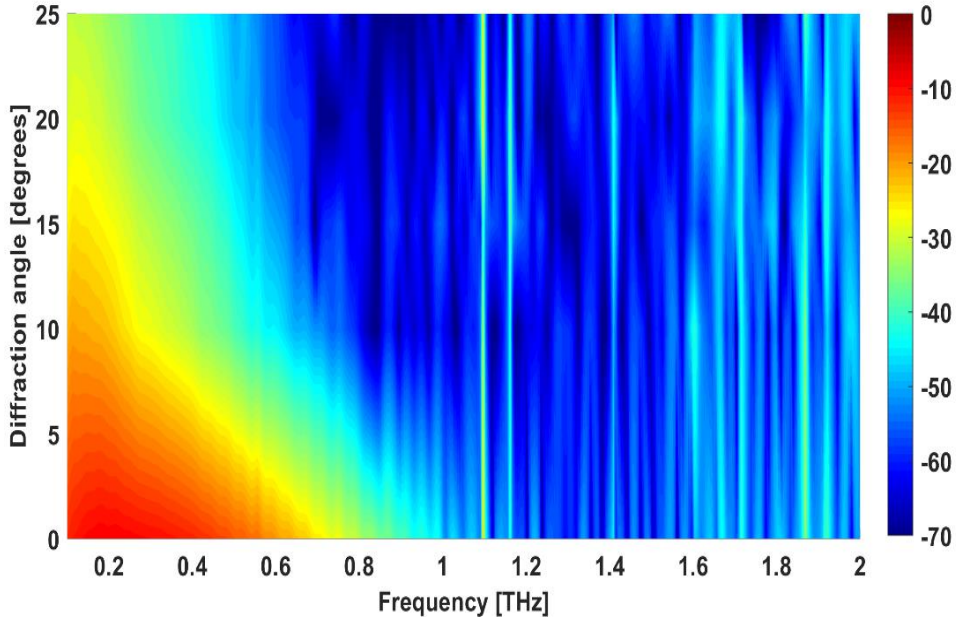

Figure 38. Jointly measured knife-edge effect.

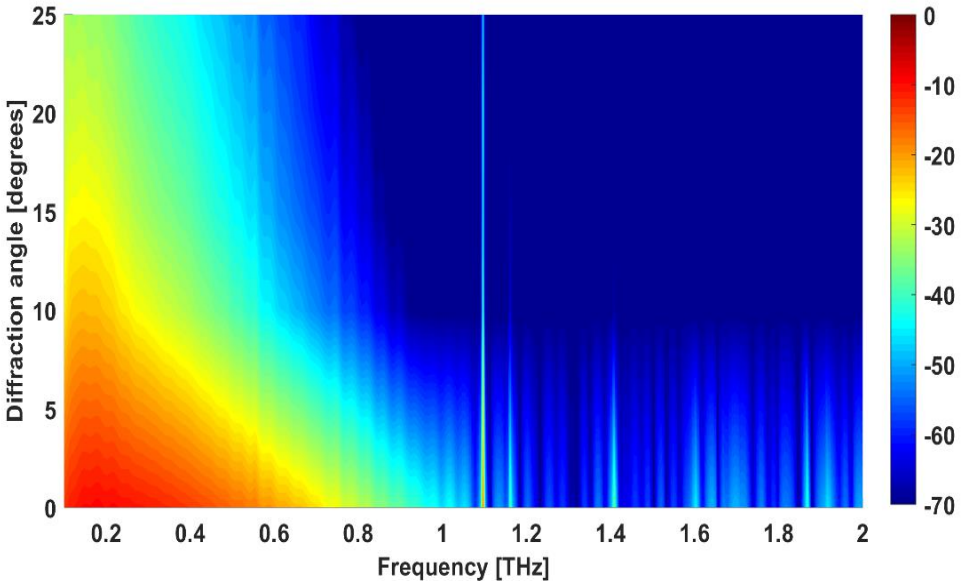

Figure 39. Calculated knife-edge effect.

The pulse shape of the jointly measured multipath effect is shown in Figure 40. The figure shows the results as a function of the frequency and energy of the received signals. It gives a very good illustration that the signal dissipates more energy at higher frequencies and becomes weaker with the increase of diffraction angle. The signal is getting noisy at around 1 THz.

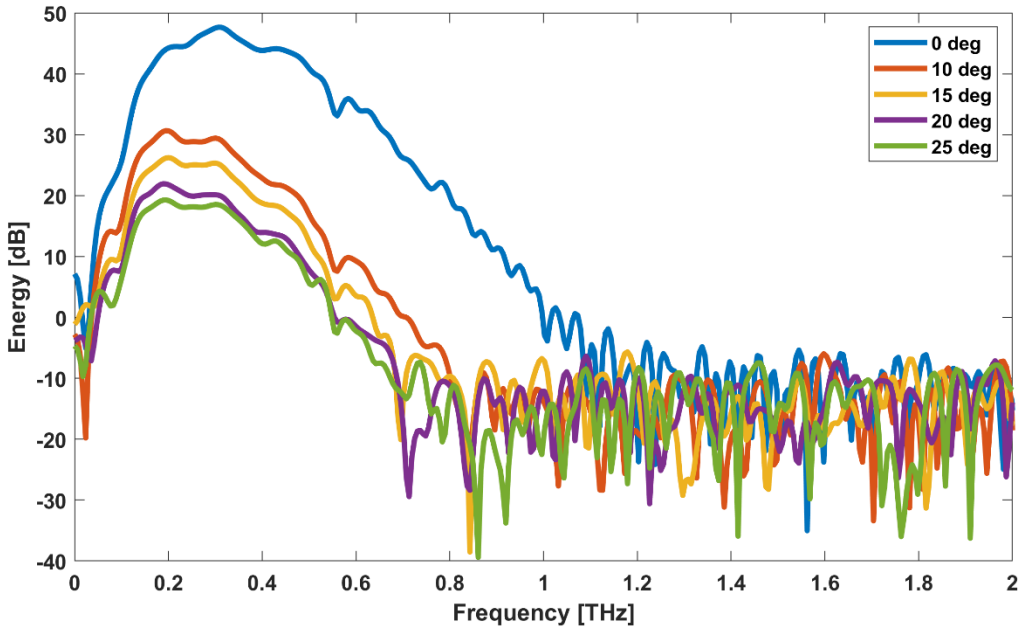

Figure 40. Pulse shape of jointly measured knife-edge effect.

5.5.2.2 Single Slit Effect

The following two figures (Figures 41 and 42) show the jointly measured response and calculated single slit diffraction effect of two individually taken measurements respectively, discussed in Sections 5.1 and 5.4.2. The measurement setup has been given in the previous

chapter. Figures are limited from 0.1 to 2 THz. Here, we get very little response at the receiver. Two separately taken measurements have shown a reasonable match. The responses remain very weak in both cases. The blue color indicates the complete noise portion. Despite that, it still possible to get response up to 0.7 THz when the signal experiences at least two NLOS components. However, it is uncertain that the response might be either the message signal or ISI.

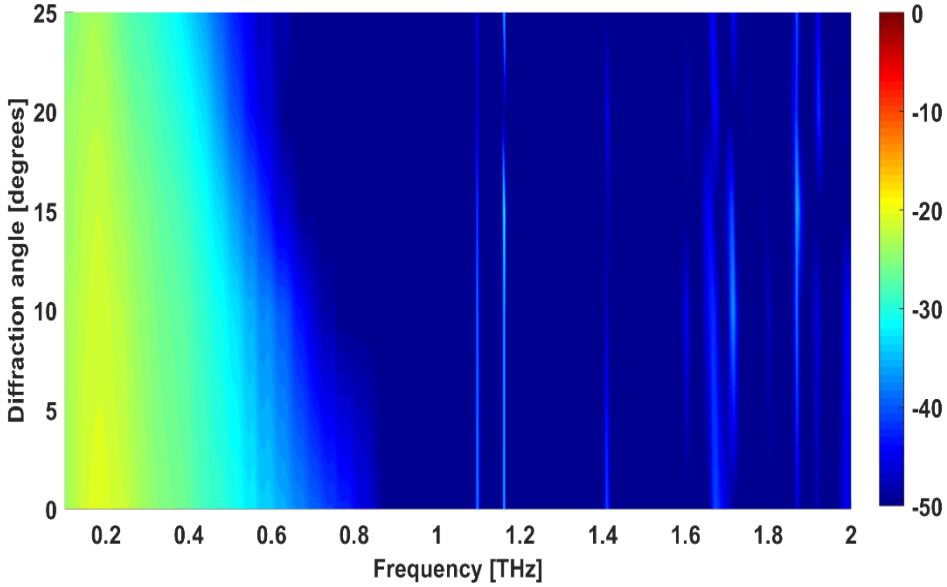

Figure 41. Jointly measured multipath single slit effect.

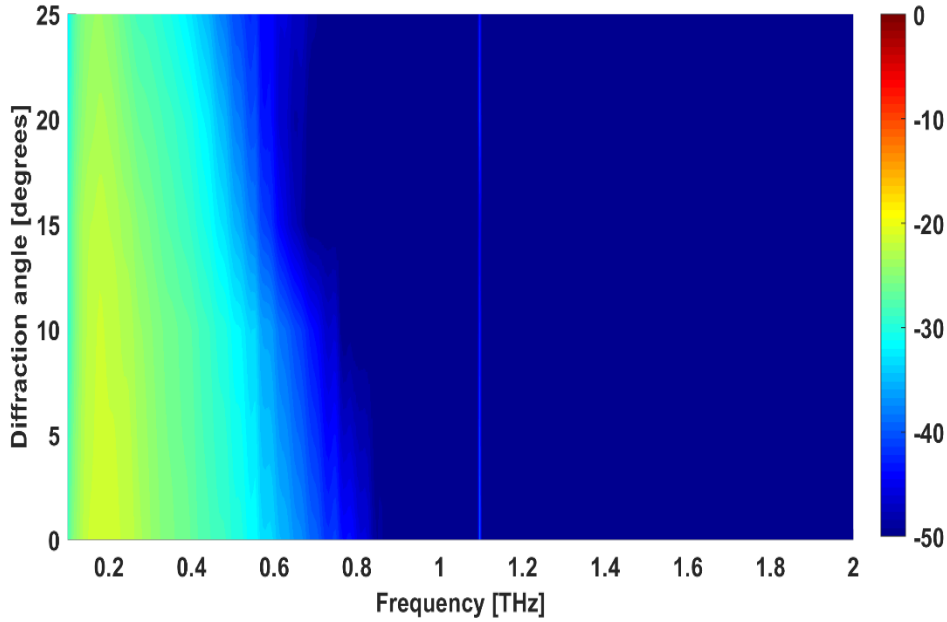

Figure 42. Calculated multipath single slit effect.

Figure 43 shows the single slit effect as a function of frequency and energy. The figure shows that with the increase of frequency offset and angles, the signal attenuates more. The most

reliable path can be obtained at lower angles only. The path gain drops significantly at high frequency because of frequency selective fading.

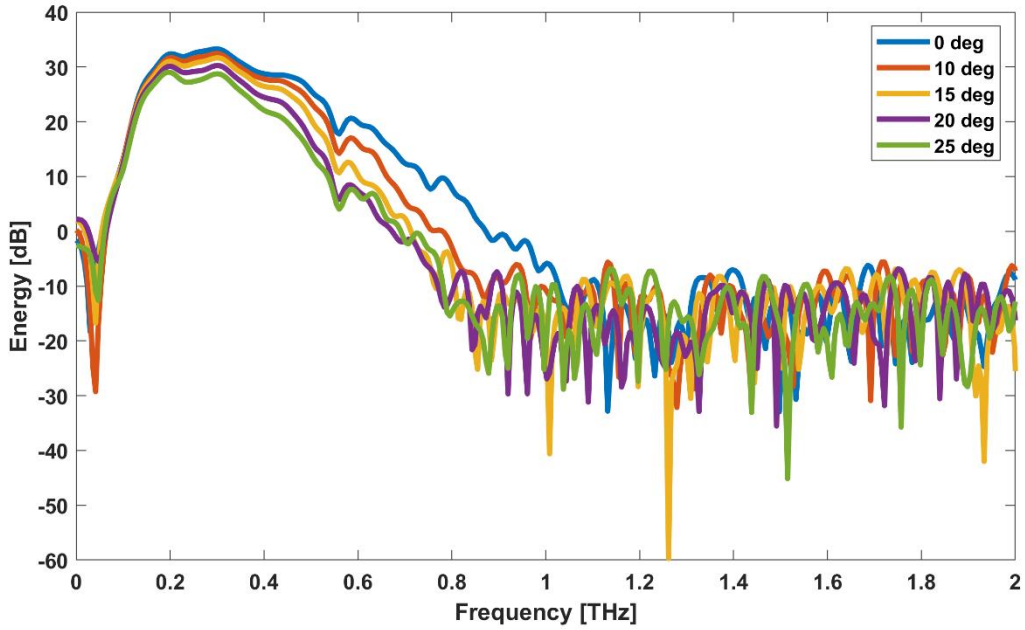

Figure 43. Pulse shapes of jointly measured single slit effect.

5.6 Discussion

The measurement results of three types of wave propagation mechanisms, including reflection, diffraction, and penetration, have been reported in this work. We verified and compare our measurement results data with the theory discussed in the third chapter. Firstly, we have presented the measurement results of the penetration loss of three different materials at the beginning of Section 5. We also calculated the penetration coefficient of these materials. The information about the penetration coefficient give us information to predict the reflection and transmission properties of the THz wave. The refractive index for the three dielectric materials over several frequency bands ranging from 300 GHz to 900 GHz has been reported. However, materials characterization was needed to design and estimate the multipath propagation model in the case of penetration, reflection, and diffraction phenomena. In our case, the value of the refractive index decreases when we move from lower frequencies to higher frequencies.

The penetration results showed that glass allows more penetration amongst the three materials. The results also showed that the materials allow penetration up to roughly 1.5 THz. In higher frequency, the signal attenuation is very high, and most of the high frequency components has been filtered out over 1 THz for all the three samples. It is possible to communicate through the penetrated path but it's true for only in the lower portion of the THz band [15], [16].

Secondly, we have also reported the measured results of reflection attenuation measurements of four different materials, including aluminum, glass, plastic, and thick hardboard. Our key focus was to predict the specular reflection properties of these materials. The scattering loss has also affected the received signal, depending on the roughness of the surface. Despite that, this phenomenon not solemnly studied in this thesis. Scattering from the surface of the material was highly dependent upon the smoothness of the surface of the materials. Materials used in the measurement were not perfectly polished. In our case, aluminum was the only sample used

where penetration of the THz wave was uncertain. This sample was a non-coated metal sheet, so it does not allow penetration on its surface. On the other hand, all the other three samples allow some sort of penetration on the material's surface. We have presented the individually taken measurement results first. Hence, aluminum reflects the radiation very well. The specular reflected path was the strongest path. The results were quite reasonable at lower reflections angle up to 2 THz in the experiment. It is also true for all the metal to some extent, which does not allow penetration on its surface. Metal could be an excellent reflector at lower reflection angles. Moreover, the glass and plastic do allow penetration on their surface. So, the radiation is not fully reflected back to the receiver as some energy might be penetrated through the medium. Also, there was existing scattering loss on the surface as the surface was not smothered enough. On the contrary, the hardboard does allow absorption and scattering on its surface, but the reflected path gains at lower angle offsets up to 1 THz were tolerable. The signal attenuates more at higher reflection angles and frequency offset for all the materials [14].

Thirdly, the diffraction pattern of terahertz wave is very much well fitted with our modified theory specifically for knife-edge diffraction. Our measurement shows a good possibility for communicating in the THz wireless channel by the diffracted path with reasonable signal attenuation. It is valid for lower diffraction angles only. The path gain drops to near noise level with the increase of the diffraction angles. It might be suggested from the experiment that knife-edge diffraction could be an option in wireless communication as it gives most of the information at very low angles and with shorter distances. The attenuation might go higher if the distance is getting longer. The diffracted path always adds delay to the receiver end as the wave travels longer distances, especially in the NLOS situation. The single slit measurement is not very common in wireless communication. It does not offer a well-diffracted path as much as a knife-edge diffracted path does [21].

Another important part was to make a comparison of the two diversely designed multipath propagation models built to analyze the THz channel behavior. Theoretically, both the multipath gain of two distinct models would have similar responses, but the inequality comes from various aspects. It also depends upon the ambient environment of the room for each measurement. The path losses came from the molecule absorption because of the water vapor exists in the lab room. This is one of the distinct features of the THz frequency that it is sensitive to ambient humidity and temperature. The THz band is strongly affected by the molecule absorption loss [23]. The absorption is also dependent on the distances, as discussed in Section 3.1.

The jointly measured response of two NLOS components has been reported in this thesis for four different materials. The comparison of the single NLOS component to the jointly measured NLOS components also reported. We have separately taken the measured response for single NLOS phenomena; reflection or diffraction first after that multiplied the individually taken penetrated path gain through thin hardboard with either reflection or diffraction measurement results. Then compare the calculated results with completely distinguish NLOS scenarios where a combination of penetrated and reflected or diffracted path gain measured simultaneously. The two NLOS scenarios with different samples were well-matched as anticipated. The path gain is significantly weaker as the signal experiences penetration and reflection losses along with other losses in the communication channel. The longer distance causes additional delay to the transmitted signal at the receiver. The tolerable path gains can only be achievable at lower reflection or diffraction angles and lower frequency offset [14]-[23].

6 SUMMARY

The thesis studied various NLOS propagation mechanisms in the terahertz frequency band by different measurement techniques. Several dielectric samples were used in the experiments. The feasibility of NLOS multipath has been analyzed to estimate the possible THz communications link. The results have been reported from 0.1 to 3 THz in most cases. Several NLOS components such as reflection, diffraction, penetration, and combination of those phenomena were analyzed empirically as well as theoretically. All the measurements were conducted at the University of Oulu's communication laboratory. The results fit well with the corresponding theories.

Despite that, there were many challenges too. The accuracy of the measurement setup should be taken care of very carefully to get better measured responses. The TeraView TeraPulse 4000 measurement device used for taking the measurement has highly directional beam. Therefore, sample placement was cautiously taken care of while taking measurements. Every sample was adjusted to both vertical and horizontal positions correctly. Any displacement or inaccuracy might affect the received signal significantly at the receiver end, especially for the higher frequency portion of the THz regime. The dielectric samples characterization was also a bit challenging. To find the effective refractive indices for each sample over several frequency bands was difficult to fit with the Fresnel equations because of the refractive indices on the surface of the measured dielectric materials were unknown. We used to follow the method of curve fitting with the Fresnel equation to the measured responses, which is challenging for the frequency above 1 THz. Matlab software has been used throughout the process, from extract data to calculation and plotting the desired results.

From our findings, the overall NLOS multipath environment is very much possible in the THz regime. Most of the earlier papers suggested that the single NLOS phenomena might be very reasonable for the THz band communication. This thesis paper investigated that the signal could propagate through any dielectric materials and then experience another NLOS propagation mechanism, including reflection or diffraction, before reaching the receiver. It can be said that the signal can still be received after multiple NLOS phenomena occurred in the wireless channel. Thus, it offers an overall decent multipath environment. The received signal attenuation is tolerable up to 1 THz in the case of multiple NLOS phenomena. It can be expected that the communication can only be possible at lower reflection or diffraction angles. The message signal contains ISI or interference and attenuates exponentially when the frequency goes higher above 1 THz.

Therefore, it is inevitable that the THz regime of the electromagnetic spectrum is an excellent choice for short-distance wireless communications. It can be possible that this high frequency band can be used to set up a communication link between the emitter and receiver antenna after the signal propagates through multiple NLOS components. It is noteworthy that this band offers very large bandwidth with ultra-high-speed communication. Due to its high free space path loss, it might be used for indoor communications with high gain antennas. The possibilities are very extensive, and the feasibility of this such high frequency is still at the research level. This massive bandwidth of the THz band might be the obvious choice for the deployments of the state-of-the-art wireless communication technology beyond 5G.

7 REFERENCES

[1] Christian Jansen, Radoslaw Piesiewicz, Daniel Mittleman, Thomas Kürner & Martin Koch (May 2008) The Impact of Reflections From Stratified Building Materials on the Wave Propagation in Future Indoor Terahertz Communication Systems, IEEE Transactions on Antennas and Propagation, Vol. 56, No. 5.

[2] Ian F.Akyildiz, Shuai Nie, Shih-Chun Lin & Manoj Chandrasekaran (2016) 5G roadmap: 10 key enabling technologies. Elsevier Computer Networks Vol. 106:17-48.

[3] Thomas Kürner & Sebastian Priebe (2014) Towards THz Communications-Status in Research, Standardization and Regulation, Journal of Infrared, Millimeter, Terahertz Waves 35, 53-62.

[4] George R. MacCartney, Theodore S. Rappaport (July 2019) Millimeter-Wave Base Station Diversity for 5G Coordinated Multipoint (CoMp) Applications, IEEE Transactions on Wireless Communications, Vol. 18, No. 7, pp. 3395-3410.

[5] International Telecommunication Union Report (2017), Minimum Requirements Related to Technical Performance for IMT-2020 Radio Interface(s), Retrieved May 24, 2020, from http://www.itu.int/pub/R-REP-M.2410

[6] Ian F.Akyildiz, Josep Miquel Jornet, Chong Han (2014) Terahertz Band: Next Frontier for Wireless Communications, Physical Communication 12: 16-32.

[7] Kao-Cheng Huang & Zhaocheng Wang (5 May 2011) Terahertz Terabit Wireless Communication, IEEE Microwave Magazine 1527-3342.

[8] Russell Ford, Menglei Zhang, Marco Mezzavilla, Sourjya Dutta, Sundeep Rangan and Michele Zorzi (13 March 2017) Achieving Ultra-Low Latency in 5G Millimeter Wave Cellular Networks, IEEE Communications Magazine, Vol:55, No:3, pp:196-203.

[9] Juho Lee, Younsun Kim, Yongjun Kwak, Jianzhong Zhang, Aris Papasakellariou, Thomas Novlan, Chengjun Sun, Yingyang Li (March 2016) LTE-advanced in 3GPP Rel-13/14: an evolution toward 5G, IEEE Communications Magazine, Vol. 54, No. 3, pp. 36-42.

[10] Theodore S. Rappaport, Yunchou Xing, Ojas Kanhere, Shihao Ju, Arjuna Madanayake, Soumyajit Mandal, Ahmed Alkhateeb, Georgios C. Trichopoulos (2019) Wireless Communications and Applications Above 100 GHz: Opportunities and Challenges for 6G and Beyond, IEEE Access, Vol. 7, pp. 78729-78757.

[11] Naoya Kukutsu & Yuichi Kado (March-2009) Overview of Millimeter and Terahertz Wave Application Research, NIT Technical Review, Japan, Vol. 7, No.3.

[12] Ian F.Akyildiz & Josep Miquel Jornet (2010) The internet of nano-things, IEEE Wireless Communications Magazine, Vol.17, No.6: 58-63.

[13] Xi-Cheng Zhang & Jingzhou Xu, Introduction to THz Wave Photonics, New York, Springer.

[14] Joonas Kokkoniemi, Janne Lehtomäki, Vital Petrov, Dmitri Moltchanov, Yevgeni Koucheryavy & Markku Juntti (2016) Wideband Terahertz Band Reflection and Diffuse Scattering Measurements for Beyond 5G Indoor Wireless Networks, In: Proc. European Wireless, pp. 1-6.

[15] Joonas Kokkoniemi, Janne Lehtomäki, & Markku Juntti (2016) Measurements on Penetration Loss in Terahertz band, In: Proc. European Conference Antennas Propagation, pp. 1-5.

[16] Joonas Kokkoniemi, Janne Lehtomäki, Vital Petrov, Dmitri Moltchanov & Markku Juntti (2016) Frequency Domain Penetration Loss in the Terahertz Band, In: Proc. Global Symp. Milli. Waves, pp. 1-4.

[17] Sebastian Priebe, Christian Jatrow, Martin Jacob, Thomas Kleine-Ostmann, Thorsten Schrader, & Thomas Kürner (May 2011) Channel and Propagation Measurements at 300 GHz. IEEE Transactions on Antennas and Propagation, Vol. 59 No.5.

[18] Christian Jansen, Sebastian Priebe, Christoph Möller, Martin Jacob, Hanno Dierke, Martin Koch & Thomas Kürner, (2011) Diffuse Scattering From Rough Surfaces in THz Communication Channels. IEEE Trans. THz Sci. Technol. Vol. 1, No. 2:462-472.

[19] Joonas Kokkoniemi, Janne Lehtomäki & Markku Juntti (2018) Reflection Coefficients for Common Indoor Materials in the Terahertz Band, 1-6. 10.1145/32331888.3233204.

[20] Radoslaw Piesiewicz, Christian Jansen, S. Wietzke, Daniel Mittleman, Martin Koch & Thomas Kürner (2007) Properties of Building and Plastic Materials in the THz Range. Int. J Infrared Milli. Waves Vol. 28, No. 5, pp. 369-371.

[21] Joonas Kokkoniemi, Perttu Rintanen, Janne Lehtomäki, & Markku Juntti (2016) Diffraction Effects in Terahertz Band-Measurements and Analysis, In: Proc. IEEE Global Commun. Conf., pp. 1-6.

[22] Sayed Amir Hoseini (November 2017) A Theoretical Study of the Effect of Molecular Absorption and Re-radiation on Millimeter-Wave and Terahertz Wireless Networking, Doctor of Philosophy in Computer Science and Engineering, The University of New South Wales, Australia

[23] Josep Miquel Jornet & Ian F. Akyildiz (2011) Channel Modeling and Capacity Analysis for Electromagnetic Wireless Nanonetworks in the Terahertz Band, IEEE Trans. Wireless Commun. 10 (10) 3211-3221.

[24] Recommendation ITU-R P.526-13: Propagation by Diffraction, International Telecommunication Union Radio Communication Sector (ITU-R) Std.

[25] Simon R. Saunders & Alejandro Aragon Zavala (2007) Antennas and Propagation for Wireless Communication System (Second edition), John Wiley & Sons, Ltd.

[26] H. D. Young and R. A. Freedman (2012) Sears & Zemansky's University Physics: with Modern Physics (13th Edition), A. Black, Ed. Addison Wesley.

[27] S.Popa, N.Draghiciu & R. Reiz (2008) Fading Types in Wireless Communications System, Faculty of Electrical Engineering and Information Technology, University of Oradea. 1.

[28] Sanjiv Kumar, P.K. Gupta, G. Sing & D. S. Chauhan (2013) Performance Analysis of Rayleigh and Rician Fading Channel Models Using Matlab Simulation, I.J. Intelligent Systems and Applications, MECS URL:(http://www.mecs-press.org/).

[29] Marvin K. Simon & Mohamed-Slim Alouini (2002) Digital Communication over Fading Channels- A Unified Approach to Performance Analysis, John Wiley & Sons Inc, Online ISBN: 9780471200697.

[30] Phillips C., Parr J. & Riskin E. (2013) Signals, Systems and Transforms. Pearson Education.

[31] Ian F. Akyildiz, Chong Han & Shuai Nie (2018) Combating the Distance Problem in the Millimeter-Wave and Terahertz Frequency Bands, IEEE Communications Magazine (Volume: 56, Issue: 6), DOI: 10.1109/MCOM.2018.1700928.

[32] P. Boronin, D. Moltchanov & Y. Koucheryavy (2015) A Molecular Noise Model for THz Channels, IEEE International Conference on Communication (ICC), London, pp. 1286-1291.

[33] Joonas Kokkoniemi, Janne Lehtomäki, & Markku Juntti (2016) A Discussion on Molecular absorption noise in the Terahertz Band, Elsevier Nano Commun. Networks J. 8: 35-45.

[34] A. Douplik, G. Saiko, I. Schelkanova & V. V. Tuchin (2013) Lasers for Medical Applications-The response of tissue to laser light (Third Chapter), Woodhead Publishing Series in Electronic and Optical Materials, Pages 47-109.

[35] J. D. Parsons (2011) The Mobile Radio Propagation Channel, John Wiley and Sons Ltd. Second Edition, DOI: 10.1002/0470841524.

[36] M. Rieche, A. Ihlow, T. Heyn, F. Pérez-Fontán & G. Del Galdo (2015) Land mobile satellite propagation characteristics from knife-edge diffraction modeling and hemispheric images, 9th European Conference on Antennas and Propagation (EuCAP), Lisbon, pp. 1-4.

[37] Christopher Haslett (2008) Essentials of Radio Wave Propagation, Cambridge University Press.

[38] Dr. Richard Rudd, Dr. Ken Craig, Dr. Martin Ganley & Richard Hartless (2014) Building Materials and Propagation-Final Report, Ofcom.

[39] Alexander I. Lvovsky (2013) Encyclopedia of Optical Engineering, Taylor and Francis: New York, Chapter Fresnel Equations, 1-6.

[40] Louis Desmarais, Applied Electro Optics (1997), Pearson Education.

[41] Balanis C.A. (2005), Antenna Theory-Analysis and Design. John Wiley & Sons Inc., Second Edition.

[42] Dr. M.N. Avadhanulu & Dr. P.G. Kshirsagar (2008), A Textbook of Engineering Physics. S. Chand & Company Pvt. Ltd.

[43] Andreas F. Molisch (2010) Wireless Communications, John Wiley & Sons, Ltd., Second Edition.

[44] Chong Han, Josep Miquel Jornet and Ian F. Akyildiz (12 November, 2012) Statistical Multi-path Propagation Modeling and Fading Analysis in Terahertz Band Communication Networks, URL:(https://mentor.ieee.org/802.15/documents?is_group=0thz), Accessed 24 February, 2020.

[45] Antti V. Räisänen and Arto Lehto (2003) Radio Engineering for Wireless Communication and Sensor Applications, Artech House, Inc.